2017

Characterization of MALT1 Inhibitors and Their Effect on Leukemic Cell Growth Properties

Christina Snyder
Rowan University

CHARACTERIZATION OF MALT1 INHIBITORS AND THEIR EFFECT ON LEUKEMIC CELL GROWTH PROPERTIES

Christina Snyder, B.E.

A Dissertation submitted to the Graduate School of Biomedical Sciences, Rowan University in partial fulfillment of the requirements for the M.S. Degree.

Stratford, New Jersey 08084

March 2017

Table of Contents Page

Acknowledgements

I would like to express my gratitude to my research mentor Dr. Ilana Stroke for her continued guidance in the completion of my thesis project. I would like to acknowledge Dr. Rachael Siegel for her day to day mentorship and support both on and off the bench. The advice given to me by Dr. Stroke and Dr. Siegel has been indispensable, both for my project and for my future career in research. I would also like to thank Dr. Lyndi Rice for the initial development of my project, mentorship early in the project, and for helping me develop basic laboratory skills.

I would like to thank Dr. Grant Gallagher for his support through the course of the program and his dedication to creating a challenging and fun learning environment. I would like to thank the members of my thesis advisory committee, Dr. Jason Trama, Dr. Joseph Nickels, and Dr. Salvatore Caradonna for their assistance in the progression and completion of my thesis. I would especially like to thank Dr. Joseph Nickels for his invaluable support and guidance. I am grateful to all of the members of Venenum Biodesign, LLC and Oncoveda, of Genesis Biotechnology Group, for welcoming me into their community and sharing their wealth of wisdom.

I would like to thank Dr. Diane Worrad, the Rowan University Graduate School of Biomedical Science, and Genesis Biotechnology Group for facilitating my thesis research. Lastly, I am grateful to Dr. Eli Mordechai and Dr. Martin Adelson for providing the opportunity, funding, and space required for my thesis research to ensue.

Abstract

Leukemia is the most common childhood cancer, with a combined 40,000 predicted new cases in the United States in 2016 [8]. The two most common subtypes are acute myeloid leukemia (AML) and chronic lymphocytic leukemia (CLL) [9-11]. The commercially available inhibitor of Bruton's tyrosine kinase (BTK) has shown promising results in clinical trials for CLL because of the importance of BCR signaling in CLL [12-15]. Recent studies suggest that the outgrowth of BTK inhibitor resistant clonal cells in some CLL patients results in a treatment-refractory phenotype [16-18]. MALT1, a protein involved in BCR activation of the NF-κB pathway that functions downstream of BTK, is a promising new target aimed at treating an aggressive BCR signaling-dependent subtype of non-Hodgkin's lymphoma, known as ABC-DLBCL [1-3, 6]. Targeting this protein for small molecule inhibition may be effective in the treatment of BTKi-refractory CLL patients, as well as other leukemias, such as AML [19]. The effect of MALT1 or BTK inhibition on AML, CLL, and DLBCL cell proliferation was analyzed. Together with examination of protein expression in each cell line and the effect of MALT1 inhibition on cleavage of its downstream target RelB, it is supported that a clinical MALT1 inhibitor would be effective in slowing the growth of CLL, ABC-DLBCL, and AML tumors. Combinatorial experiments supported the hypothesis that combination treatment with MALT and BTK inhibitors could be efficacious at treating patients with relapsed or refractory CLL or ABC-DLBCL.

Introduction

Leukemia Burden on Society

Chronic lymphocytic leukemia (CLL) is the most common type of leukemia in adults in the United States. Approximately six of every hundred thousand males will be diagnosed with CLL in the U.S. this year [10]. CLL patients on average spend fifty-thousand dollars more in medical care over their lifetime than people without the disease [20]. This is due to the increased frequency of inpatient hospital stays and necessary high cost pharmaceuticals. The chronic nature of CLL creates long term financial stress for patients and their families. The estimated burden on society is 340 million dollars per year [20]. Richter's transformation occurs in fifteen percent of patients with CLL, and the patients die within two to three years of diagnosis. The transformation causes the leukemic cells to develop into diffuse large B-cell lymphoma (DLBCL), an aggressive form of non-Hodgkin's lymphoma (NHL) that is associated with a poor prognosis. Thirty percent of patients have a more passive variety and die from causes unrelated to CLL. The remaining majority of patients undergo five to ten years of latent disease, followed by periods of active disease, treatment, and relapse, ultimately leading to a CLL-related death [17]. Current therapy for CLL includes a combination of chemotherapy and immunotherapy. Targeting B cells with anti-CD20 antibodies has induced remission in some patients for up to five years when used together with alkylating agents such

as chlorambucil. Following treatment, relapse usually occurs due to mutations affecting p53, a tumor suppressor protein [21].

Acute myeloid leukemia (AML) is the second most common type of leukemia in adults in the United States and accounts for twenty percent of all childhood malignancies [22]. Within five years of diagnosis, 73.4% of patients will die from AML or treatment related causes. In the first six months after diagnosis, patients may have combined treatment costs as high as $350,000 for chemotherapy and stem cell transplantation [23]. The current standard of care for treating AML is chemotherapy, radiation therapy, or stem cell transplant [9]. All of these treatment methods are extremely invasive, expensive, and debilitating, and although they may increase the life expectancy of AML patients, the treatment is not curative and the patient's quality of life is diminished.

Diffuse large B-cell lymphoma (DLBCL) is an aggressive type of NHL that accounts for twenty-five percent of all NHL cases [2]. NHL is the seventh most common cancer, with an estimated seventy-thousand new cases in 2016 nationwide [24]. First line therapy for DLBCL includes CHOP chemotherapy (cyclophosphamide, doxorubicin, vincristine, and prednisone); however patient relapse or refractoriness is common [25]. Costs associated with aggressive NHL may be up to $15,000 per month [26].

Chronic Lymphocytic Leukemia (CLL) Pathophysiology

CLL tumor cell survival is dependent on B-cell receptor (BCR) activation and downstream signaling of various proliferative pathways, including NF-κB and AKT/mTOR [21, 27]. Essential proteins involved in BCR signal transduction include PI3K, MALT1, BTK, ERK, and IKK (Fig. 1). In a normal B-cell, somatic hypermutation of the immunoglobulin (Ig) variable (V) region is crucial for affinity maturation and the production of a useful BCR. It has recently been identified as a prognostic marker for CLL tumor behavior. Unmutated Ig-V typically indicates malignancy earlier in B-cell development and is correlated with a more aggressive phenotype [27, 28]. Targeting proteins downstream of the BCR for small molecule inhibition may be successful in the treatment of patients with CLL due to the tumor's dependence on BCR signaling.

Acute Myeloid Leukemia (AML) Pathophysiology

AML develops when a clonal population of myeloid stem cells proliferate and differentiate abnormally [29]. Three types of genetic mutations are commonly seen in AML and correlate with different prognoses. Class I mutations typically activate pro-proliferative pathways, and must occur together with class II mutations, which impair normal hematopoietic differentiation. Common class I mutations include FLT3, K/NRAS, TP53, c-KIT, and STAT3. Common class II mutations include NPM1 and CEBPA. Class III mutations are involved in epigenetic regulation, or mutations in proteins that are involved in DNA histone tail methylation, including DNMT3A, TET2, and IDH-1/2 [29]. Targeting proteins within the pathways that these mutations affect may be a successful approach to treatment of patients with

AML. Although AML cell survival is not dependent exclusively on NF-κB signaling, recent evidence has shown that targeting proteins in the NF-κB pathway, such as BTK, could be efficacious in treating AML patients [19].

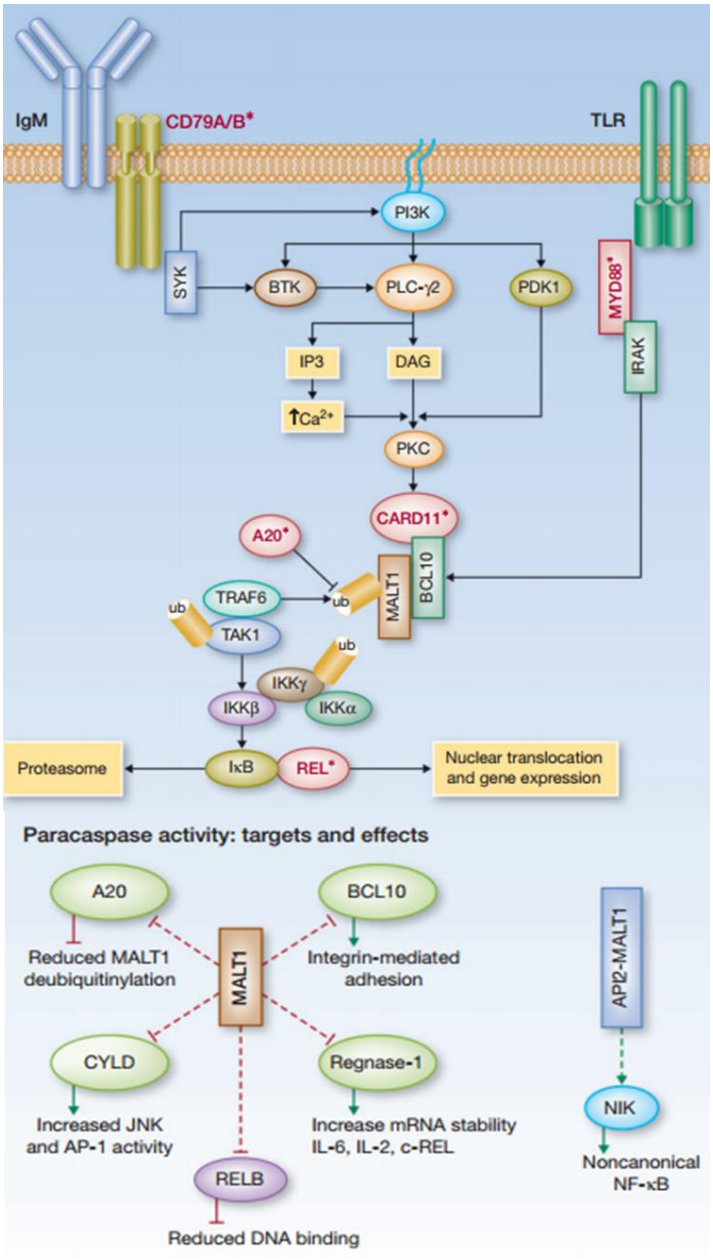

Figure 1. MALT1 and BTK in NF-κB signaling. MALT1 activates canonical NF-κB signaling through activation of IκB kinase and cleavage of its target proteins downstream of the BCR, TCR, or TLR. BTK is activated downstream of the BCR in order to activate NF-κB, Ras, and JNK signaling. [1]

Diffuse Large B-Cell Lymphoma (DLBCL) Pathophysiology

DLBCL is classified into three subtypes, including activated B-cell like (ABC), germinal center B-cell like (GCB), and primary mediastinal B-cell like (PMBL). These subtypes differ in mechanisms of pathogenesis, frequency of specific oncogenic mutations, and responsiveness to certain treatments. Patients with the ABC subtype commonly have a worse prognosis than do patients with other subtypes due to a lack of effective treatment options.

ABC-DLBCL is characterized by constitutively activated BCR signaling. This is most commonly due to mutations in BCR components, including CD79A and CD79B. The mutations usually occur in the immune receptor tyrosine activation motif (ITAM) [30]. This domain contains a phosphorylation site for SYK, a downstream negative regulator of the BCR. The mutation prevents BCR signal termination and internalization, resulting in constitutively activated NF-κB. Another common mutation in ABC subtype tumors is in CARD11, a binding partner in the CARD11-BCL10-MALT1 (CBM) complex downstream of the BCR (Fig. 1). This mutation spontaneously initiates binding with MALT1 and BCL-10, and thus enhances the NF-κB signal [31]. Cell lines that are known to contain CARD11 mutations (OCI-LY3) or CARD11 wild type protein (U-2932) were investigated in order to examine the relationship between this mutation and inhibition of various proteins in the pathway [32].

Unlike ABC-DLBCL, GCB subtype tumors have not been shown to rely on chronic active BCR signaling for their survival. Recently, sequencing studies have shown mutations in *Rel* and *Pten* genes in GCB-type tumors but not ABC-type

tumors [33]. *Rel* gene amplifications allow for a more robust NF-κB response in tumor cells by increasing production of NF-κB proteins. PTEN inactivation may play an important role in GCB tumor progression. As a tumor suppressor, PTEN works to inhibit activation of Akt by PI3K. When PTEN is inactivated, over-activation of Akt results in cell growth, protein synthesis, and resistance to apoptosis [34]. Overexpression of the microRNA mir-17-92 has also been seen in GCB-DLBCL. Mir-17-92 has been shown to induce the overexpression of MYC and resultantly reduce apoptosis of malignant cells [33].

Mucosa-Associated Lymphoid Tissue 1 (MALT1) Structure and Function

Mucosa-Associated Lymphoid Tissue 1 (MALT1) is a paracaspase that is involved in the normal immune response through classical NF-κB signaling by mitogenic activation of the BCR or T cell receptor (TCR). Upon BCR or TCR stimulation BTK is activated, which leads to the activation of protein kinase C (PKC) and the phosphorylation of (Caspase recruitment domain-containing protein 11) CARD11. CARD11 then recruits MALT1 and B-cell lymphoma protein 10 (BCL10) to form the CARD11-BCL10-MALT1 (CBM) complex (Fig. 1). Once bound, MALT1 serves as a scaffolding protein and recruits the E3 ligase TNF receptor associated factor 6 (TRAF6) to facilitate the polyubiquitination of MALT1 on lysine 63. As a result, the inhibitor of κB kinase (IKK) is recruited to the complex and activated by TAK1. Activated IKK phosphorylates the inhibitor of the κB protein (IκB-α), resulting in the ubiquitination and degradation of the inhibitory protein. This allows the now liberated NF-κB transcription factor proteins to translocate into the

nucleus, specifically p50, p52, RelA/p65, RelB, and c-Rel [6, 35-37]. The migration of NF-κB proteins initiate the expression of genes involved in T and B cell proliferation and growth, maturation and class switching of immunoglobulin receptors, upregulation of various cell adhesion molecules, expression of apoptosis regulatory proteins, and expression of certain growth factors and their receptors [38].

MALT1 is unique in that in addition to its scaffold function, it functions as a paracaspase, cleaving proteins that are involved in the regulation of NF-κB signaling (Fig. 1). MALT1 is the only human paracaspase. It differs from caspases in that it cleaves its substrates after arginine as opposed to aspartic acid [39]. Caspase-dead MALT1 is able to propagate the NF-κB signal, but not as robustly as when it is able to cleave its target proteins, indicating that its paracaspase function is crucial for proper immune cell function and growth. Identified substrates of MALT1 include RelB, A20, CYLD, Regnase-1, Roquin-1 and -2, and BCL 10 [34]. RelB and A20 are negative regulators of NF-κB that are cleaved by MALT1. RelB forms a complex with the RelA and C-Rel proteins, prohibiting transcription of their target genes. Upon cleavage at arginine 85 by MALT1, RelB is degraded by the proteosome and RelA and C-Rel are free to initiate transcription [6, 40]. A20 inhibits NF-κB as a part of the normal negative feedback mechanism of NF-κB signaling in many cell types. It does so by de-ubiquitinating various proteins upstream, including TRAF6, MALT1, and IKKγ, thus reducing IKK and TRAF6 binding to the CBM complex. Upon cleavage by MALT1, the ability of A20 to de-ubiquitinate its targets is diminished and the NF-κB signal is enhanced. Upon cleavage by MALT1, CYLD likely promotes AP-1 family transcription factor activation, including c-Jun and c-Fos, thus

enhancing lymphocyte differentiation and proliferation and inhibiting apoptosis [6]. Regnase-1 and Roquin-1 and -2 are endonucleases that have been shown to cleave the 3' untranslated region (UTR) of mRNA, resulting in destabilization of the mRNA and decreased target protein expression [41]. Specifically, *Il16, Il12b, Il2, Ctla4, Icos,* and *Rel* (encoding c-Rel protein) mRNA are modified by Regnase-1 and *Tnf* mRNA is modified by Roquin [42]. These mRNAs encode proteins involved in propagation of the NF-κB signal**.** Upon cleavage by MALT1, Regnase-1 and Roquin are unable to cleave their mRNA targets, and the above listed mRNAs are able to be translated. The effect of Bcl-10 cleavage on NF-κB signal regulation is unclear, but this cleavage event has been shown to upregulate T cell adhesion to fibronectin. It is likely that other MALT1 target proteins exist that further modulate the NF-κB signal. The ultimate effect of MALT1's proteolytic activity is the enhancement of NF-κB signaling.

MALT1 contains three domains that are critical for its function, including a death domain (DD), immunoglobulin domains (Ig), and a caspase-like domain (Fig. 2). Critical for the scaffolding function of MALT1 are the Ig domains, which allow for BCL-10 and TRAF6 binding and the K63-linked polyubiquitination that is responsible for IKK recruitment and activation. The caspase-like domain contains catalytic sites for cleavage of RelB, A20, CYLD, and other MALT1 substrates. Recently, an autoprocessing site at arginine 149 was discovered that results in cleavage of MALT1's death domain. Although it is known that this autoprocessing enhances the NF-κB signal, the mechanism of action is unknown.

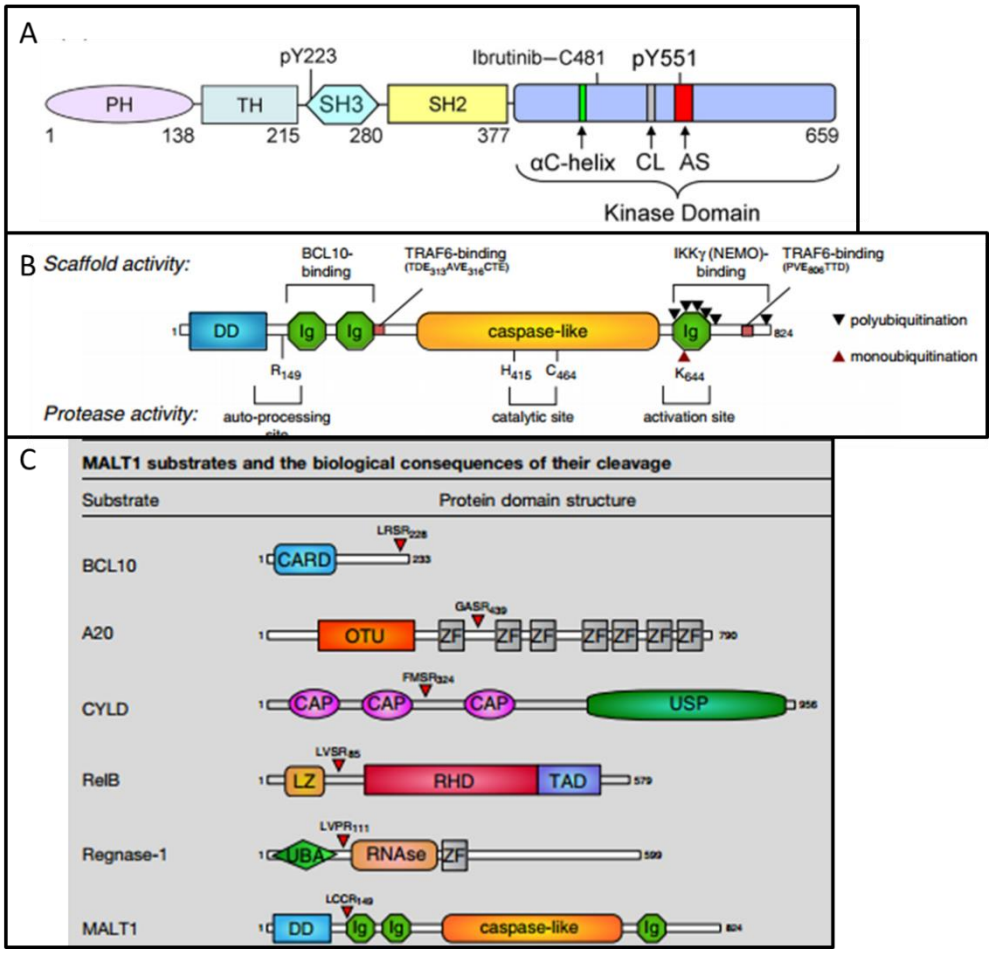

Figure 2. Domain structures of BTK, MALT1, and MALT1 substrates. A) The domain structure of BTK shows the pleckstrin homology (PH), Tec homology (TH), Src homology 3 (SH3), Src homology 2 (SH2), and Src homology 1/tyrosine kinase (SH1/TK) domains. Regions of significance are shown, including the Ibrutinib binding site at cysteine 481 and activation and transactivation sites at tyrosine 223 and tyrosine 551. B) The domain structure of MALT1 shows a death domain (DD), Immunoglobulin-like domains (Ig), and a caspase-like domain. Crucial sites for the scaffold function (top) are shown, including the BCL-10, TRAF-6, and IKKγ binding sites. Ubiquitination sites are shown as triangles in the relevant regions. Crucial sites for MALT1's protease activity (bottom) are shown, such as the site for activation, its catalytic site, and an auto-processing site. C) Domain structures of MALT1 substrates are shown. Cleavage sites are indicated by a red triangle. [6, 7]

MALT1 as a Cancer Drug Target

Various mutations that affect proteins involved in NF-κB signaling, such as MyD88, CARD11, A20, and CD79B are commonly seen in lymphomas and leukemias, including ABC-DLBCL, CLL, MCL, and acute lymphoblastic leukemia (ALL) [3, 6, 43]. These mutations affect both positive and negative regulators of the pathway, ultimately resulting in constitutive activation of the NF-KB signal. CARD11 mutations, seen in some ABC-DLBCL tumors, prevent inactivation of CARD11 and allow binding of the CBM complex without antigenic stimulation, resulting in constitutively activated NF-κB signaling. More commonly seen in ABC-DLBCL tumors and other B-cell malignancies are CD79B mutations. CD79B is a component of the BCR that binds Lyn kinase after receptor stimulation to negatively regulate the signal. Mutations in CD79B prevent Lyn kinase activity following receptor stimulation and result in a prolonged downstream signal [6].

MALT1 is a promising therapeutic target for multiple leukemia and lymphoma subtypes such as DLBCL, CLL, AML, and MALT lymphoma. This is because of its critical role in NF-κB signal propagation and in NF-κB pathway dependent tumor growth. MALT1 functions downstream of many common activating mutations in the pathway, as described above. Inhibition of MALT1 would allow for downregulation of the NF- κB signal even when mutations in CARD11, CD79, or MyD88 are present. To date, mutations in MALT1 have not been described in lymphoma.

Inhibition of MALT1

Inhibition of MALT1 can be achieved using various commercially available inhibitors [1-3, 35]. The small molecule non-competitive reversible inhibitors of MALT1, mepazine hydrochloride and thioridazine hydrochloride (Fig. 3), were recently discovered by D. Nagel's laboratory in Neuherberg, Germany using a fluorescent peptide cleavage assay [3]. The phenothiazines, including mepazine and thioradizine, were originally discovered as dopamine D2 receptor antagonists and were used as anti-psychotics and sedatives. This class of compounds has been shown to induce extrapyrimidal side effects, including varying degrees of muscle spasms, rigidity, and tremors [44]. A tetrapeptide inhibitor (z-VRPR-Fmk) binds and inhibits MALT1 in vitro at low nanomolar concentrations, but is unsuitable for cell-based or clinical experiments due to poor cell penetrance and pharmacokinetics. A small molecule irreversible protease inhibitor, MI-2, was discovered using a cell-based proliferation inhibition assay, and further characterized by a MALT1 cleavage assay by Western blot (Fig. 3) [2]. The compound has been shown to bind the caspase domain of MALT1, inhibit the growth of ABC-DLBCL cell lines, and inhibit the cleavage of CYLD [2]. It is anticipated that a novel small molecule inhibitor of MALT1 would be effective in slowing tumor growth of ABC-DLBCL and other hematologic malignancies where BCR activation and NF-κB signal propagation is involved, such as CLL or AML.

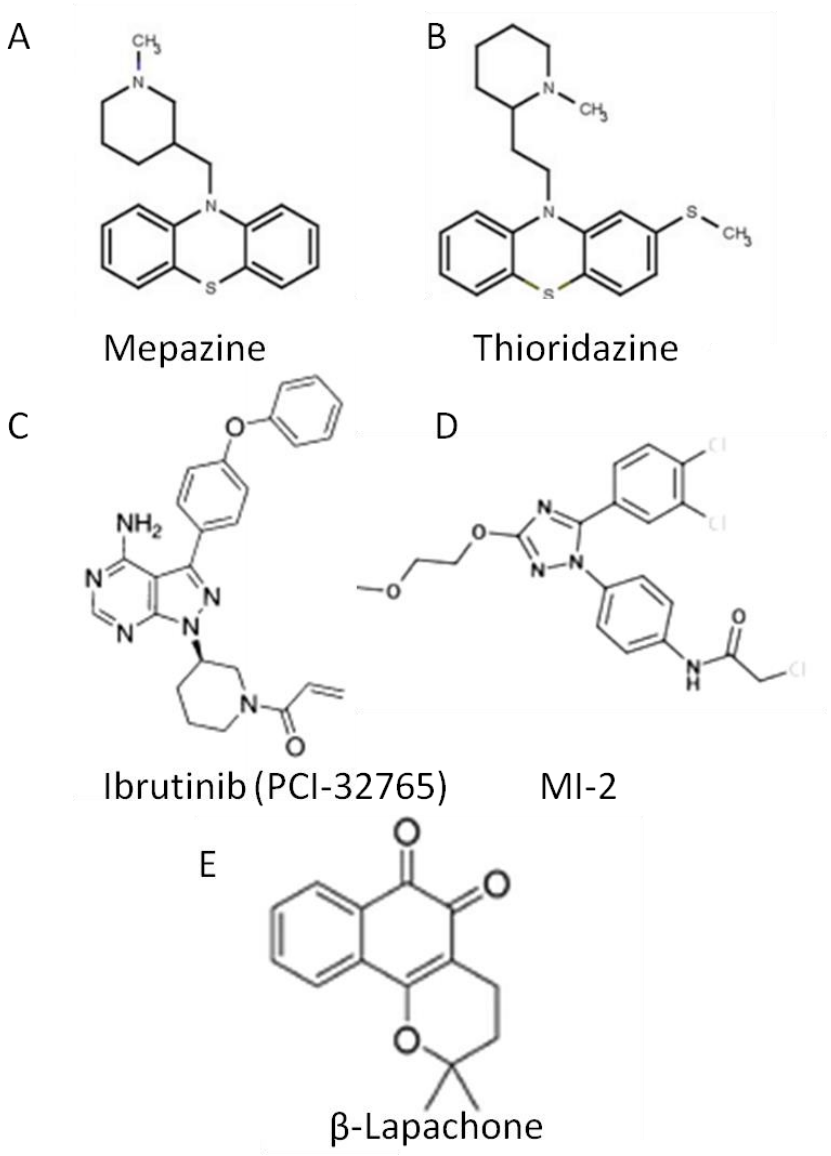

Figure 3. Structure of MALT1 and BTK inhibitors. A, B) Mepazine and thioridazine, both noncompetitive reversible inhibitors of MALT1, are shown. C) The structure of Ibrutinib (PCI-32765), an irreversible allosteric inhibitor of BTK, is shown. D) The structure of MI-2, an irreversible inhibitor that binds and inhibits the paracaspase activity of MALT1 is shown. E) The structure of β-Lapachone, a small molecule inhibitor of MALT1. [2-5]

Bruton's Tyrosine Kinase (BTK) Structure and Function

Bruton's tyrosine kinase (BTK) is a non-receptor cytoplasmic protein that is crucial for BCR signaling and B cell adhesion. It is encoded by the XLA gene and is a member of the Tec family of protein kinases [45]. It consists of pleckstrin homology (PH), Tec homology (TH), Src homology 3 (SH3), Src homology 2 (SH2), and Src homology 1/tyrosine kinase (SH1/TK) domains (Fig. 2) [45]. BTK is expressed primarily in maturing B- cells, and can also been seen in myeloid progenitor cells. Important functional sites of BTK are present in the PH domain, including the binding site of phosphatidylinositol-3,4,5-triphosphate (PIP_3), a phospholipid that activates BTK, and the binding site for inhibitor of BTK (IBTK). Trans-phosphorylation initially activates BTK in the activation loop located in the SH1/TK domain. Subsequently, auto-phosphorylation occurs in SH2 and SH3 domains. Nuclear export and localization sequences are located in the SH2 and SH3 domains, which is required for nuclear-cytoplasmic transport of BTK.

BTK has been shown to contribute to signaling from receptors other than the BCR, such as TLRs, RANK, FcRIII, and CXCL12 [46]. This may be why inhibition of BTK has been efficacious in treating tumors that do not rely exclusively on BCR signaling for their survival, such as AML. Upon BCR stimulation, the phosphorylation of CD19 by SYK results in the activation of PI3Kδ, which generates PIP_3. PIP_3 binds BTK and the complex localizes to the plasma membrane. BTK is trans-phosphorylated at tyrosine 551 by SYK, then auto-phosphorylated at tyrosine 223 to become activated. Once active, BTK activates PLCγ2, which indirectly activates Ras/MAPK, Rap1, IKK, and JNK signaling. Diacylglycerol (DAG) and

inositol-1,4,5-triphosphate (IP_3) are produced by PLCγ2, activating PKC and its various downstream targets, including NF-κB signaling (Fig. 1) [12, 15, 17].

Inhibition of BTK

BTK has been shown to be crucial for CLL and MCL tumor cell survival and is overexpressed and constitutively phosphorylated in AML [19]. Knockdown of BTK using shRNA in AML cell lines impairs cell growth, suggesting that BTK is important for AML cell survival [47]. Inhibition of BTK using an orally bioavailable small molecule inhibitor (Ibrutinib) is effective in treating patients with relapsed CLL and MCL.

Ibrutinib (PCI-32765, Pharmacyclics/Janssen) is a small molecule inhibitor of BTK that covalently and irreversibly binds to cysteine 481 with a half maximal inhibitory concentration (IC_{50}) of 0.5 nM in a biochemical kinase assay (Fig. 3) [5]. The compound selectively binds to the SH1/TK domain of BTK at an allosteric site and prevents full activation by blocking auto-phosphorylation at tyrosine 223. In CLL and MCL, Ibrutinib inhibits ERK and NF-κB activity, promotes Caspase-3 dependent apoptosis, inhibits DNA replication, and delays disease progression. In preliminary in vitro studies, Ibrutinib inhibits the growth of some AML cell lines [47]. The compound is generally non-toxic [45] to normal T cells and has shown promising preclinical and clinical results in patients with CLL and MCL due to the importance of BTK and BCR signaling in the pathogenesis of CLL and MCL [5, 12, 48, 49]. Other orally bioavailable small molecule inhibitors targeted for BTK are

being investigated for the treatment of CLL, MCL, AML, DLBCL, multiple myeloma, and rheumatoid arthritis [45, 50].

Resistance to BTK Inhibitor Therapy

Normal and cancerous B-cells are under constant pressure to produce a working BCR and remain active and dividing. This process is known as affinity maturation. The nature of this selection process allows for some cancerous B-cells to mutate into clones that are resistant to BTK inhibitor (BTKi) therapy [21, 27]. In a minority of patients who undergo Ibrutinib therapy, accumulation of resistant clonal cells results in overall phenotypic resistance to Ibrutinib and patient relapse. It has been suggested that resistance to Ibrutinib can be conferred by mutations that activate NF-κB signaling downstream of BTK. An activating mutation in PLCγ2, a downstream substrate of BTK, as well as a mutation at cysteine 481 of BTK have been reported in patients with post-BTKi-treatment relapse [17]. Activating mutations in other proteins that are downstream of BTK, such as CARD11 and BCL10, confer non-responsiveness to BTKi therapy. Mutations in SF3B1, Notch1, and BIRC3 are also associated with refractoriness in patients with CLL, although the mechanism is unknown [51]. MALT1 inhibitor therapy independently or in combination with BTK inhibitors, may be effective in treating patients who have relapsed following BTK inhibitor treatment because it functions downstream of BTK, PLCγ, CARD11, and BCL10.

High Throughput Screening and MALT1 Drug Discovery Efforts

Current efforts to develop a small molecule inhibitor targeted for MALT1 are underway by several teams. Several articles cite the importance of BCR signaling in DLBCL, CLL, and other B-cell malignancies, and propose targeting a protein downstream of the receptor in order to treat patients with these disorders [1, 27, 28]. MALT1, BTK, PI3K, and SYK inhibitors have been proposed and developed with the goal of treating BCR dependent malignancies [30]. The tool compounds Mepazine and MI-2 have been crucial in the development of novel high throughput screening (HTS) assays to examine compound effectiveness on a large scale. Monitoring of the protease activity of MALT1 is an effective way to analyze inhibition of MALT1 by potential inhibitors. Venenum Biodesign, LLC has developed a MALT1 specific biochemical assay that was then used for a HTS with the goal of discovering novel inhibitors of MALT1. A substrate of MALT1 was conjugated with a rhodamine fluorophore when upon cleavage by MALT1 produces a fluorescent product. Higher fluorescence is correlated with more substrate cleavage and higher activation of MALT1 enzyme. A library of 6 million small molecule compounds was screened using the assay, and the structure activity relationship of potential hits is currently being examined. Similar assays have been developed for MALT1 small molecule inhibitor screening, including at Medivir (Huddinge, Sweden), Novartis (Ambler, PA, USA), Astra Zeneca (Mölndal, Sweden), and by Daniel Nagel at the Helmholtz Zentrum München–German Research Center for Environmental Health, Institute of Molecular Toxicology and Pharmacology (Neuherberg, Germany) [3, 52-54]. A

Fluorescence Resonance Energy Transfer (FRET) reporter assay using the interaction between YFP and CFP has also been developed for MALT1 and may be used for screening compounds [55]. Non-HTS methods of evaluation may be performed on a smaller scale to evaluate cell based compound effectiveness and downstream effector functions. This includes qRT-PCR or ELISA to monitor IL-6 production, Western blotting to analyze RelB, CYLD, and A20 cleavage and the phosphorylation of IKBα, and phenotypic assays monitoring proliferation or migration [6].

Rationale

There is a need for a more effective treatment that targets the molecular mechanisms responsible for CLL, AML, and DLBCL tumorigenesis and metastasis. Current treatments non-specifically target rapidly dividing cells or remove the cells entirely by bone marrow transplant. These debilitating and costly treatments reduce the patient's quality of life and often come with complications and side effects. Targeting a protein by small molecule inhibition downstream of the BCR may be effective in slowing the growth of various B-cell malignancies. MALT1 is a promising drug target for many tumors that rely on constitutive activation of the BCR or NF-κB signaling. A novel small molecule inhibitor targeted for MALT1 may be effective at treating the ABC-subtype of DLBCL.

Inhibition of BTK by small molecules has been revolutionary in the treatment of CLL. However, due to the nature of B-cell malignancies the accumulation of mutations conferring resistance to efficacious BTK inhibitors have become increasingly common in patients being treated for CLL. Most frequently, mutations downstream of BTK constitutively activate the NF-KB pathway. Targeting a protein downstream of BTK, such as MALT1, could augment BTK inhibitor therapy in patients who have become resistant to treatment. Although AML cells are known to not rely completely on NF-κB signaling, recent evidence has shown that inhibition of NF-κB pathway proteins slows tumor cell growth.

In order to investigate the relationship between commercially available MALT1 and BTK inhibitors and their effect on cell proliferation and pathway

activation, first, biochemical characterization of MALT1 inhibitors was necessary because of limited reliable data on the inhibitors. Subsequently, DLBCL, CLL, and AML cell lines were chosen for characterization of compounds in cell-based assays, based on their expression of the target proteins MALT1 and BTK, effect of inhibition on pathway activation downstream, and dependence on MALT1 for growth. These factors were investigated through a few crucial experiments, including a cell proliferation assay, examination of cleavage of the MALT1 substrate RelB, and drug combination experiments. The proliferation of each cell line was monitored using an ATP detection system and the effect of MALT1 or BTK inhibitors on cell growth was examined. Combination experiments using a MALT1 and BTK inhibitors were completed in order to determine possibly synergy between compounds. The effect of MALT1 inhibition on the cleavage of RelB, a direct downstream target of MALT1, was monitored by western blot. Together the experiments served to provide information that is important for the development of new treatments for lymphoma and leukemia patients.

Materials and Methods

Mepazine was acquired from EMD Millipore and Ibrutinib from Selleck Chemicals. MI-2 and z-VRPR-Fmk were acquired from Tocris Bioscience. Thioridazine and β-Lapachone were acquired from Sigma Aldrich. Compounds A and B were discovered at Venenum Biodesign through a HTS for a MALT1 inhibitor. Assay plates were acquired from Greiner. Unless specified, buffer components were acquired from Sigma Aldrich. All cell growth media and its components, including fetal bovine serum (FBS) and penicillin-streptomycin solution, were acquired from Corning.

Biochemical Assays

MALT1 Fluorescence Assay

Mepazine, MI-2, thioridazine, and β-Lapachone were dissolved in DMSO to a starting concentration of 10 mM. Because of the difference in potency of the peptide inhibitor in comparison to the small molecules, Z-VRPR-Fmk was diluted more than the other compounds, to a starting concentration of 41 µM. 20 µL of each compound was added to the first column of a 96-well U-bottom plate, where each compound was placed in its own row. 20 µL DMSO was added to columns 2-12 of the plate. 10 µL of diluted compound from column 1 was added to column 2. This was continued to column 11, creating a 1:3 serial dilution of compounds. Column 12 contained DMSO only as a blank. 8µL of each compound dilution was transferred to an acoustic source plate, a black 384-well clear bottom, small volume, low base plate. An acoustic dispenser was used to dispense 40 nL of each compound dilution to a

384-well high base, low volume black plate. Final compound concentrations of mepazine, MI-2, thioridazine, and β-Lapachone ranged from 40 μM to 0.67 nM. Final compound concentration of z-VRPR-Fmk ranged from 165 nM to 2.8 pM.

Assay buffer consisted of 200 mM Tris HCl (pH 7.5), 800 mM sodium citrate, 1 mM DTT, 0.1 mM EGTA, 0.05% CHAPS. The pH of the buffer was readjusted to 7.5 before use. Human recombinant MALT1 enzyme (Origene) was diluted in assay buffer to 4 nM and was added to each well for a final concentration of 2 nM of enzyme. A substrate of MALT1 tagged with rhodamine (Ac-LRSR-Rh110-Dpro) (Biosyntan) was diluted in assay buffer with 0.01% BSA in a glass tube. 5 μL of 20 μM substrate was added to each well for a final concentration of 10 μM. Assay plates were centrifuged at 205 x G for 30 seconds and incubated with a black cover at 37°C in a humidified chamber.

Biochemical Assay Fluorescence Reading and Data Analysis

After 1, 1.5, 2, 3, and 4 hours incubation, the plate was read using a ViewLux plate reader (Perkin Elmer). The fluorophore was excited at a wavelength of 492 nm and emission was read at 529 nm. Increased fluorescence correlated with more substrate cleavage by MALT1 enzyme. Using GraphPad Prism software, fluorescence was plotted versus the logarithm of the test compound molarity (log(M)) as an average ± standard deviation. Using the software, a nonlinear regression analysis using the log(M) (inhibitor) vs. response, variable slope with four parameters conditions were used to generate an $IC_{50.}$ A graph of enzyme and substrate without test compound fluorescence over time was plotted to ensure that the signal increased steadily over time.

Thermal Melt Assay Optimization

Thermal shift assay buffer was made to include MALT1 Assay Buffer (see MALT1 Fluorescence Assay) and a final concentration of 1mM DTT or PBS + 1mM DTT. 1.5 µL of SYPRO Orange (Sigma Aldrich) protein dye was added to 1.5 mL of each buffer. 2µL of 1 µM MALT1 protein was added to reaction wells with 18 µL of assay buffer containing SYPRO Orange for a final concentration of 0.1 µM protein. Wells with buffer + dye only were included as a control. The plate was centrifuged for 30 seconds at 205 x g. A qRT-PCR instrument (Stratagene) was used to increase the reaction temperature by 1°C every 30 seconds. The reaction temperature started at 25°C and after 71 cycles ended at 96°C.

Thermal Melt Data Analysis

Data was analyzed using MxPro software (Agilent Technologies), Microsoft Excel, and GraphPad Prism. Endpoint fluorescence readings were taken at the end of every cycle, approximately every 30 seconds. Raw fluorescence values were plotted over temperature, R(t), and a derivative, R'(t),was taken using MxPro. The negative derivative, -R'(t), was calculated in Excel and plotted in Prism. Melting temperature of the protein was characterized as the maximum value of –R'(t).

Thermal Shift Assay with MALT1 Inhibitory Compounds

SYPRO Orange Dye was added to PBS + 1mM DTT to make the assay buffer as described (see Thermal Melt Assay Optimization). MALT1 protein (Origene) was added to reaction wells with 18 µL assay buffer for a final protein concentration of 0.1 µM. Compounds were diluted to 10 mM or 1 mM in DMSO, then to 1 mM or 100 µM in assay buffer. 2 µL of the compound dilutions were added to each reaction

well with or without MALT1 enzyme. Final concentrations of the compounds were 100 μM or 10 μM for Mepazine, MI-2, and Compounds A and B (Venenum Biodesign), and 4.11 μM for z-VRPR-Fmk. Wells with buffer + dye only were included as a control. A 2.5% DMSO control was included to ensure consistency with the amount of DMSO present in the peptide inhibitor samples. The plate was centrifuged for 30 seconds at 205 x g. A qRT-PCR instrument (Stratagene) was used to increase the reaction temperature by 1°C every 30 seconds. The reaction temperature started at 25°C and after 71 cycles ended at 96°C.

Cell Culture

Cell Lines and Growth Conditions

Cells were cultured in growth media recommended by the American Type Culture Collection (ATCC), supplemented with 20 % fetal bovine serum (FBS), 100 I.U. penicillin, and 100 μg/mL streptomycin at 37°C, 5% CO_2. Cell lines were purchased from either ATCC or the German Collection of Microorganisms and Cell Cultures (DSMZ). Cell lines used, media used for growth, and ATCC or DSMZ catalog numbers can be seen in Table 1.

Cell Line Name	Lymphoma or Leukemia subtype	Source (Catalog #)	Media	Concentration (20 mL culture)	Concentration (384-well Proliferation Assay)
HL-60	AML	ATCC (CCL-240)	RPMI-1640	1 x 10^6 cells/mL	6000 cells/well
MEC-1	CLL	DSMZ (ACC 497)	Iscove's DMEM	2 x 10^5 cells/mL	1500 cells/well
OCI-AML-2	AML	DSMZ (ACC 99)	α-MEM	2 x 10^5 cells/mL	1500 cells/well
OCI-AML-3	AML	DSMZ (ACC 582)	α-MEM	2 x 10^5 cells/mL	1500 cells/well
OCI-LY-3	ABC-DLBCL	DSMZ (ACC 761)	RPMI-1640	1 x 10^6 cells/mL	1500 cells/well
SU-DHL-4	GCB-DLBCL	ATCC (CRL-2957)	RPMI-1640	1 x 10^6 cells/mL	2000 cells/well
SU-DHL-6	GCB-DLBCL	ATCC (CRL-2959)	RPMI-1640	1 x 10^6 cells/mL	2000 cells/well
U-2932	ABC-DLBCL	DSMZ (ACC 633)	RPMI-1640	2 x 10^5 cells/mL	3000 cells/well

Table 1. Cell lines used. Cell lines used and their associated source and catalog number, lymphoma or leukemia subtype, growth media as suggested by ATCC, concentration for re-suspension of continuing culture, and concentration for seeding in a 384 well-plate.

Cell Line Maintenance

Cells were split every two to three days as determined by color change in the media and visual inspection with a microscope. Since all cell lines are non-adherent, no trypsinization was needed to remove cells from the flask. Cells were removed from their flask or plate, placed in a 50 mL conical tube, and centrifuged for 5 minutes at 250 x g to pellet cells. The media was aspirated off the cell pellet, 7 mL of fresh media was added, and cells were resuspended gently by pipetting. Cells were counted according to the protocol detailed below and resuspended in a 75 mL flask in 20 mL at the desired cell density (Table 1).

Counting cells

After cells were pelleted and resuspended in fresh media, 5 µL of the cell solution was mixed with 10 µL sterile PBS and 5 µL Trypan Blue solution (Corning). 10 µL of the mix was pipetted into a disposable Hemocytometer (InCyto). Two of the four corner boxes were visualized using a microscope (Olympus) at 10X magnification. The cells within the corner boxes were counted, and the average of the boxes was taken. The average was multiplied by 4×10^4 due to the dilution factor of the hemocytometer and initial dilution. The resulting number represents the number of cells/mL in the cell solution. Volume needed for resuspension of the cells at the desired concentration was calculated.

Freezing cells

Cells were counted according to the protocol detailed above and pelleted by centrifugation to contain 1×10^6 cells. Cells were resuspended in 1 mL of freezing medium, which contained 95% complete growth medium and 5% DMSO (Sigma

Aldrich), and was transferred to a cryogenic vial (TPP). The vial was placed in a Mr. Frosty freezing container (Thermo Fisher Scientific) and placed at -80°C to ensure a consistent cooling rate of -1°C/minute. After 24 hours, the cells were placed in the vapor phase of a liquid nitrogen tank for long term storage.

Thawing cells

5 mL of cell growth medium, supplemented with 20% serum, 100 I.U. penicillin, and 100 µg/mL streptomycin was placed in a small flask and warmed at 37°C, 5% CO_2 for thirty minutes. After warming the medium, the vial of frozen cells was incubated at 37°C for approximately five minutes, or until the entirety of the vial was defrosted. The contents of the vial was placed in the warm medium, and placed back at 37°C, 5% CO_2 for 24-48 hours or until the color of the growth medium changed or the cells reached a density of 2 x 10^6 cells/mL. If the cells did not grow significantly within 48 hours, the cells were pelleted, resuspended in fresh medium, and incubated for another 48 hours in a small flask. Once a density of 2 x 10^6 cells/mL was reached, the cells were transferred to a 75 mL flask and split as normal (see Cell Line Maintenance).

Protein Extraction and Quantification

Protein Lysate Preparation

Cells were seeded in 6-well plates at a concentration of 1 x 10^6 cells/mL in 2 mL of medium per well. After two to three days, cells were removed from the wells, centrifuged for 5 minutes at 250 x g to pellet the cells, and the media was removed. The pellet was resuspended in 500 µL sterile phosphate buffered-saline (PBS)

(Corning) by gentle pipetting. The cells were again centrifuged for 5 minutes at 250 x g. After aspiration of PBS, the pellet was resuspended in 100 µL radioimmunoprecipitation (RIPA) buffer (Cell Signaling) + Protease inhibitor cocktail (Sigma Aldrich), sonicated for 30 seconds, incubated on ice for 15 minutes, and centrifuged at 16,300 x g for 15 minutes. The lysate was either used for quantification by BCA Assay or stored at -20°C for future use.

Protein Quantification by BCA Assay

Protein was quantified using the Pierce Bicinchoninic Acid (BCA) Assay Kit (Thermo Fisher Scientific). Bovine serum albumin (BSA) protein standards (Thermo Fisher Scientific) were prepared by diluting a 2000 µg/mL stock 1:2 with sterile water. 50 µL of the stock BSA solution was added to a 1 mL centrifuge tube. 25 µL of sterile water was added to tubes 2-11. 25 µL of diluted BSA from tube 1 was added to tube 2. This was continued to tube 10, creating a 1:2 serial dilution of BSA. Tube 11 contained sterile water only as a blank. The final concentrations ranged from 2000 µg/mL to 4 µg/mL. Working reagent (WR) was created by combining reagents A and B in a ratio of 50:1 (A:B). 200 µL WR was added to 25 µL diluted BSA standard or 5 µL unknown protein in RIPA buffer + 20 µL sterile water. 100 µL of the solution was added to a well of a 96 well clear plate in duplicate. After incubation for 30 minutes at 37°C, the absorbance at 562 nm was read on a Spectramax spectrophotometer (Molecular Devices).

Protein Concentration Calculation

Protein concentration was calculated in Microsoft Excel by creating a BSA protein standard curve. Creation of the curve entailed graphing a scatter plot of the

protein concentration of the standards on the x-axis versus the absorbance of the standards on the y-axis. A linear fit was calculated by Excel and the equation was used to convert the optical densities of the unknown samples to a concentration value.

SDS-PAGE and Western Blotting

SDS-Polyacrylamide Gel Electrophoresis

Samples were prepared to have 25 µg of protein based on their calculated concentrations by BCA Assay. Each sample had 8 µL 4X loading dye (BioRad) + reducing agent (BioRad) and 25 µg protein. Water was added to each sample so that each had a final volume of 25 µL. After boiling at 100°C for 5 min in a heating block (Biometra), 25 µL of each sample was loaded onto a 4-12% Criterion polyacrylamide gel (BioRad) with 8 µL Precision Plus Kaleidoscope ladder (BioRad). The gel was run at 150 V for approximately 1-1.5 hours using 1X XT-MES (BioRad) running buffer.

Semi-Dry Transfer

Transfer buffer was made to include 100 mL Tris-Glycine (USB/Affymetrix), 250 mL methanol, and 650 mL sterile water. The buffer was refrigerated at 4°C before use. PVDF membrane (BioRad) was prepared by briefly soaking it in methanol to activate it. A Trans-Blot SD Semi-Dry transfer cell (BioRad) was used to transfer the protein gel to the PVDF membrane. Upon completion of gel electrophoresis, the gel cassette was cracked open with manual force and cut to the appropriate size using a scalpel. Thick filter paper (BioRad) of the appropriate dimensions was soaked in transfer buffer and laid on the surface of the transfer cell.

The activated PVDF membrane was laid on top of the filter paper and the polyacrylamide gel on top of that. This was followed by an additional layer of filter paper. A roller was used to ensure that no air bubbles remained in the stack. The cover was placed on the transfer cell and the transfer was run at 15V for 30 minutes.

Western Blotting

Directly after transfer to a membrane, membranes were blocked in 5% dry milk (BioRad) diluted in Tris Buffered Saline with Tween-20 (TBS-T) (USB/Affymetrix) for 30 minutes, then incubated overnight in 1:1000 dilution of primary antibody in TBS-T. The membrane was washed in TBS-T for 5 minutes three times and incubated for 30 minutes in 1:1000 secondary antibody diluted in TBS-T. Membranes were washed in TBS-T three times for 5 minutes each before imaging. Primary and secondary antibodies and their sources are listed in Table 2.

.

Antibody	Source	Number
p-BTK (Tyr 223)	Cell Signaling	5082
BTK	Cell Signaling	8547
p-IκBα-	Cell Signaling	9246
IKBα-	Cell Signaling	9242
CYLD	Cell Signaling	8462
RelB	Cell Signaling	4922
MALT1	Abcam	ab33921
GapDH	BioRad	G9545
β-Rabbit	GE Healthcare	NA934V
β-Mouse	GE Healthcare	NA931V

Table 2. Antibodies used and their source and catalog number.

Imaging Membranes

Equal amounts of EMD Millipore's Immobilon HRP Substrate Peroxide solution and HRP Substrate Luminol solution was added to each membrane. Chemiluminescence was visualized using an ImageQuant LAS 4000 (GE Healthcare Life Sciences) imager and analyzed using ImageQuant TIL (GE Healthcare Life Sciences) software. Digital images of the protein ladder was taken and processed using the ImageQuant LAS 4000 and TIL system. Blots were washed in TBS-T a second or third time if the protein bands were unclear.

Stripping and Re-Blotting Membranes

To re-probe blots for additional proteins, the membrane was first stripped using Restore Western Blot stripping buffer (Thermo Fisher Scientific). Enough buffer was poured onto the blot to cover it completely and left on a bench top rocker for 15 minutes. The membrane was washed three times for 5 minutes each with TBS-T, then re-blocked and probed according to the protocol detailed above (see Western Blotting).

Cell Based Assays

RelB Cleavage

Cells were counted and seeded into 6-well plates at a concentration of 1 x 10^6 cells/mL in 2 mL per well. Cells were incubated at 37°C, 5% CO_2 for 24 hours. Mepazine was diluted in DMSO to 2mM or 0.5 mM in a volume of 20 µL. Addition 1: 20 µL Mepazine or DMSO was added to their respective wells (Fig. 4). After addition 1, cells were incubated at 37°C, 5% CO_2 for 4 hours. Addition 2: 2 µL of

MG-132 (10 mM, Sigma Aldrich) was added to the respective wells to a final concentration of 10 μM. After addition 2, cells were incubated at 37°C, 5% O_2 for 1 hour. Cells were collected and processed for western analysis according to the protocol detailed above (see Protein Extraction and Quantification, SDS-PAGE and Western Blotting). Membranes were probed for RelB, and GAPDH as a loading control. Antibody source and catalog numbers are listed in Table 2

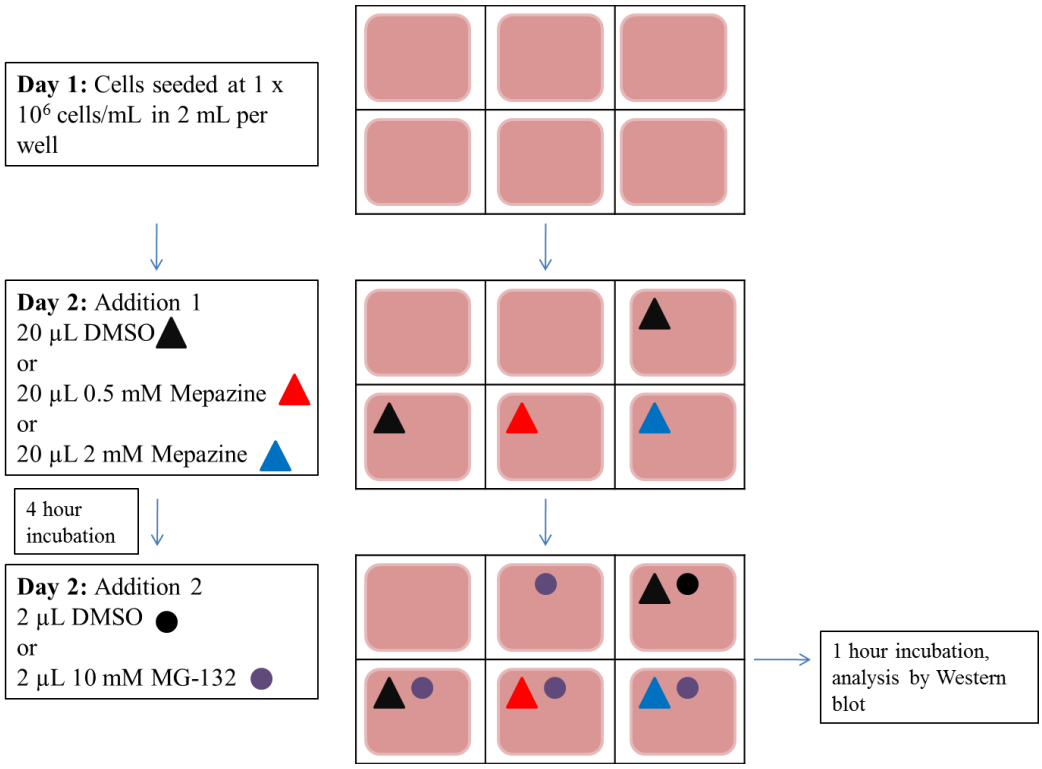

Figure 4. RelB Cleavage experiment schematic diagram. On day 1 cells were seeded at 1 x 10^6 cells/mL in 2 mL per well. On day 2, Mepazine or DMSO was added to the cells. After 4 hour incubation, the proteasome inhibitor MG-132 or DMSO was added to the cells. After 1 hour incubation, cells were processed for analysis by western blot.

Cell Titration

Cells were counted and resuspended at a concentration of 2.4 x 10^6 cells/mL in 600 µL in a 1 mL centrifuge tube, "tube 1". 300 µL of cell growth medium was added to 8 sterile tubes. 300 µL of diluted cells from tube 1 was removed and mixed with the 300 µL of media in tube 2. This was repeated to tube 8, creating a 1:2 serial dilution of cells. The lowest concentration was 19,000 cells/mL. Tube 9 contained media only and served as the blank or baseline signal. 20 µL of each cell dilution was added to three 384-well white plates (Greiner) in quadruplicate. Plates were incubated at 37°C, 5% CO_2 in a humidified chamber for 24, 48, or 72 hours.

CellTiter-Glo Luminescence Reading

After the indicated time, a plate was prepared for analysis by equilibrating the plate to room temperature for 1 hour and then adding 5 µL CellTiter-Glo (CTG) (Promega) reagent to each well (Fig. 5). The plate was spun for 30 seconds at 205 x g, placed on an orbital shaker for 15 minutes at room temperature, and spun again for 30 seconds at 205 x g. Plate luminescence was read on an Envision plate reader (Perkin Elmer). Luminescence over time or over concentration was plotted using GraphPad Prism software as the average ± standard deviation. Ideal cell number was chosen to be the least amount of cells per well, while maintaining logarithmic growth over three days, and seeing a large enough fold change in luminescence over the three day window.

Figure 5. Schematic of Cell Titer Glo ATP detection reagent. Luciferase catalyzes the conversion of luciferin to oxyluciferin and light in the presence of ATP .

Proliferation Assay with Single Agent Compounds

Ibrutinib and mepazine were dissolved in DMSO to a concentration of 50 mM in 50 µL. MI-2 and z-VRPR-Fmk were dissolved in DMSO to a concentration of 10 mM. 8 µL of each compound was added to the first column of a 96-well round bottom tissue culture plate, where each compound was placed in its own row. 4 µL DMSO was added to columns 2-11 of the plate. 4 µL of diluted compound from column 1 was added to column 2. This was continued to column 10, creating a 1:2 serial dilution of compounds. Column 11 contained DMSO only as a blank. 2 µL of this dilution was added to a new round bottom 96-well tissue culture plate. 198 µL of cell growth medium was added to mepazine and Ibrutinib rows, and 38 µL cell growth medium was added to MI-2 and z-VRPR-Fmk rows. 5 µL of the compound-media dilutions were added in quadruplicate to one 384-well white tissue culture plate. Cells were counted and resuspended at optimal concentrations determined by the cell titration assay, listed in Table 1. 20 µL of diluted cells were added to each well of the plate. Cells were incubated with compounds for 48 hours at 37°C, 5% CO_2. The plate was prepared for reading and luminescence analyzed according to the protocol detailed above (see CellTiter-Glo Luminescence Reading).

Calculation of IC_{50}

Using GraphPad Prism software, luminescence was plotted versus the logarithm of the molarity (log(M)) as an average ± standard deviation. Using the software, a nonlinear regression analysis using the log (inhibitor) vs. response, variable slope with four parameters condition was used to generate an $IC_{50.}$

Combinatorial Compound Screening Assay

Mepazine and Ibrutinib were diluted to a starting concentration of 25 mM.13µL of each compound was added to the first column of a 96-well U- bottom plate, where each compound was placed in its own row. 10 µL DMSO was added to columns 2-7 of the plate. 5 µL of diluted compound from column 1 was added to column 2. This was continued to column 6, creating a 1:3 serial dilution of compounds. Column 7 contained DMSO only as a blank. 8 µL of diluted compound was transferred to an acoustic source plate, a black 384-well clear bottom, small volume, low base plate. An ATS-100 acoustic dispenser (EDC Biosystems) was used to transfer 120 nL of compounds to a 384-well white plate in duplicate in a dose matrix (Fig. 6). Cells were resuspended at concentrations previously determined using the cell titration assay (Table 1). 30 µL of cells were added to each well of the assay plate. Plates were incubated for 2 days at 37°C, 5% CO_2 in a humidified chamber. Plates were analyzed for luminescence according to the protocol detailed above (CellTiter-Glo Luminescence Reading).

			Mepazine															
	Final concentration (uM)		cells only	100.00	33.33	11.11	3.70	1.23	0.41	0.00	100.00	33.33	11.11	3.70	1.23	0.41	0.00	cells only
			1	2	3	4	5	6	7	8	9	10	11	12	13	14	15	16
	cells only	1																
Ibrutinib	100.00	2																
	33.33	3																
	11.11	4																
	3.70	5																
	1.23	6																
	0.41	7																
	0.00	8																
	100.00	9																
	33.33	10																
	11.11	11																
	3.70	12																
	1.23	13																
	0.41	14																
	0.00	15																
	cells only	16																

Figure 6. Experimental design for matrix combinatorial experiment. Columns include a serial dilution of the MALT1 inhibitor mepazine and rows include a serial dilution of the BTK inhibitor Ibrutinib. Edge wells contained cells only to prevent evaporation of experimental well contents.

Analysis of Combinatorial Screening Assay

Single agent dilution curves were plotted as detailed in the section "Calculation of IC_{50}". Synergy between compounds was calculated using the highest over single agent (HSA) and Bliss additivism models. The HSA model uses the higher fractional inhibition of each single agent to predict the combined response. First, the raw luminescence values were calculated as an average of the fractional inhibition between 0 and 1. The larger effect of the two agents alone at each concentration was determined for each combination and subtracted from the fractional inhibition at each point in the matrix. Excess over this value was noted. The Bliss additivism model utilizes Equation 1 to predict the combined response, C, for the two single agents, A and B, represented as a fractional inhibition between 0 and 1. The observed fractional inhibition was subtracted from the predicted response in order to evaluate the excess over Bliss values [56].

Equation 1: $C = A + B - A \times B$

Transfection and Analysis

Nucleofection

To ensure consistency, cells were split on Day 1 and resuspended in 20 mL at the concentrations listed in Table 1. On day 3, cells were counted and pelleted by centrifugation for 5 minutes at 250 x g to include 2 x 10^6 cells per reaction. Each cell pellet was resuspended in 100 µL of the nucleofection buffer + supplement (Lonza: SF cell line X kit L). 2 µg pGFP plasmid DNA (Lonza) or 60 nM siRNA (GE Dharmacon: D-001630-01-05) was added to the solution. Cells were transferred to a

certified cuvette and pulsed with the EN-138 pulse on a Lonza 4D Nucleofector. Immediately after pulsation, 500 µL of the preferred pre-warmed growth medium was added to each sample, and the whole volume was transferred to 1 mL of pre-warmed growth medium in a 12-well plate. Cells were incubated at 37°C, 5% O_2 for 24 or 48 hours. After incubation for the allocated time post-transfection, cells were analyzed by Western blot or flow cytometry according to the protocols detailed in "Protein Extraction and Quantification", "SDS-PAGE and Western Blotting", and "Flow Cytometry". SiGLO and pGFP plasmid DNA transfected samples were analyzed by Flow Cytometry and MALT1 siRNA or CsiRNA transfected samples were analyzed by Western Blot.

Flow Cytometry

After 24 or 48 hours post-transfection, cells were harvested and resuspended in 100 µL PBS + 40 µL 5% paraformaldehyde (R&D Systems) diluted in PBS. Cells were stored at 4°C and analyzed within a week of collection by flow cytometry using a FACScalibur (BD Biosciences). Data was analyzed using FlowJo software (Treestar).

Results

Biochemical Characterization of MALT1 inhibitors

In order to determine the effectiveness of MALT1 inhibitors directly on MALT1 protease activity, a fluorescent biochemical assay was developed. A higher fluorescent reading correlated with higher rate of cleavage of substrate and therefore, higher activity of the enzyme. Five commercially available MALT1 inhibitors were tested along with two novel compounds that were discovered by Venenum Biodesign to inhibit MALT1 protease activity during a HTS similar to the assay described in "MALT1 Fluorescence Assay" in Materials and Methods. A 3-fold serial dilution of each compound was analyzed, and a dose response could be seen. As the concentration of inhibitor decreased, fluorescence increased in a dose-dependent manner. The fluorescence was plotted versus the logarithm of molarity, and IC_{50} was calculated (Fig. 7). Fluorescence in the presence of mepazine, MI-2, and the peptide inhibitor (z-VRPR-Fmk) (Fig. 7A), β-Lapachone and thioridazine (Fig. 7B), and the novel compound A and compound B (Fig. 7C) serial dilutions at 4 hours are shown. IC_{50}, minimum, maximum, and Hill slope values are listed in Figure 7E. Initial optimization of the assay included multiple plate readings at times ranging from 1 hour to 4 hours post-plating. Fluorescence of DMSO control wells were plotted in order to verify that a linear increase in fluorescence over time could be seen (Fig. 7D). Analysis of data points within this linear window ensures better sensitivity to inhibitors.

The peptide inhibitor had the lowest IC_{50} value (0.28 nM) and therefore, the highest potency of all the inhibitors. The dose response curves of mepazine and the peptide inhibitor were both sigmoidal in shape. A shift to the right indicates that the potency of mepazine (IC_{50}= 370 nM) is less than that of z-VRPR-Fmk. MI-2 is slightly less potent than mepazine in this assay, with an IC_{50} of 670 nM. The MI-2 curve appears different than the other two inhibitors, as it does not completely reach the "bottom" even at the highest concentration. The lowest raw fluorescence values for mepazine and the peptide inhibitor are approximately 150 and 115, respectively, at the highest concentration of inhibitor. Interestingly, the lowest raw fluorescence value that is seen for MI-2 is approximately 500, even at a high concentration of inhibitor. This indicates that there is some basal level of activity that MI-2 is unable to inhibit, and the compound does not have full efficacy in this assay when compared to Mepazine or z-VRPR-Fmk.

The inhibitors thioridazine and β-Lapachone show modest inhibition of MALT1, with IC_{50} values equal to 5 μM and 4 μM, respectively. There was more variation between replicates for these two compounds. This could be due to multiple factors such as poor solubility, aggregation, or interference with the fluorophore. It is worth noting that the compound β-Lapachone is orange in color, which could interfere with the assay. The novel compounds A and B were shown to inhibit MALT1 with IC_{50} values of 5 μM. Mepazine, MI-2 and z-VRPR-Fmk were chosen to be investigated further in future assays due to their potency (IC_{50} < 1 μM), solubility, and reliability and replicability between duplicates and experiments.

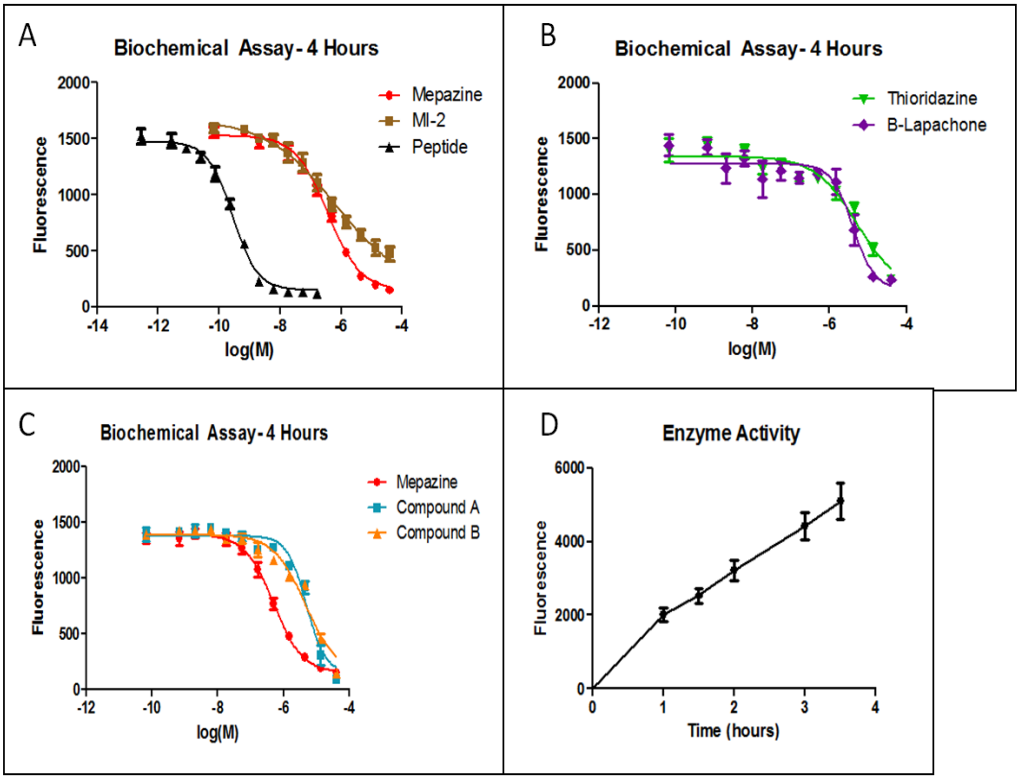

E

	Mepazine	MI-2	Peptide	Thioridazine	β-Lapachone	Compound A	Compound B
Bottom	= 150.0	= 150.0	= 150.0	= 150.0	= 150.0	= 150.0	= 150.0
Top	1529	1673	1474	1340	1276	1380	1389
LogIC50	-6.434	-6.174	-9.55	-5.29	-5.385	-5.31	-5.342
HillSlope	-0.8106	-0.3795	-1.059	-0.8039	-1.544	-1.511	-0.9159
IC50	3.68E-07	6.70E-07	2.82E-10	5.13E-06	4.12E-06	4.90E-06	4.55E-06
R square	0.9832	0.955	0.9866	0.9216	0.85	0.9677	0.9596

Figure 7. Biochemical characterization of MALT1 inhibitors using a fluorescent peptide cleavage assay. A) Dose response curves of mepazine, MI-2, and the peptide inhibitor (Z-VRPR-Fmk). B) Dose response curves of thioridazine and β-Lapachone. C) Dose response curves of compounds A and B. D) Enzyme activity over time was monitored by plotting DMSO control well fluorescence. E) Non-linear regression analysis was completed with variable slope and four parameters. Top, bottom, IC_{50}, R^2, and Hill slope values for all dose response curves. Each graph is a representative experiment of three experiments with similar results.

Thermal Melt of MALT1 Enzyme

In order to confirm that MALT1 inhibitors bind MALT1 enzyme directly, a thermal melt experiment was performed. Upon temperature increase, MALT1 protein denatures and hydrophobic pockets become exposed. SYPRO orange dye binds these residues and fluoresces. When compound binds MALT1, the protein may be stabilized to heat. This can be observed as an increase in peak fluorescence during melting. Raw fluorescence was monitored and plotted versus temperature [R(t)]. A derivative of the raw amplification plots, R'(t), was taken (Fig. 8A and 8B). The negative of the derivative, -R'(t), is shown in Figure 8C.

Optimization of assay buffer was critical for proper binding and melting of the enzyme with and without compounds. A buffer containing sodium citrate, Tris, DTT, BSA, EGTA, and CHAPS, known as MALT1 assay buffer, was compared to a buffer containing only PBS and DTT. A melt curve, R'(t), of the buffers alone without any protein can be seen in Figure 8A. Without any MALT1 protein added, the MALT1 assay buffer has its own unique thermal melt signature, while the PBS buffer remains flat. Therefore, it is not unexpected that the addition of 100 nM MALT1 protein induces a clean melting curve only in the PBS buffer, while the MALT1 assay buffer melt artifact is predominant. Labeled on Figure 8A are the peaks associated with two buffer components that were found to interfere with assay, BSA and CHAPS (data not shown). R'(t) of MALT1 protein in MALT1 assay buffer or PBS buffer can be visualized in Figure 8B. –R'(t) of the PBS buffer with and without MALT1 protein

can be seen in Figure 8C. According to the result, the melting temperature of MALT1 is 49.2°C.

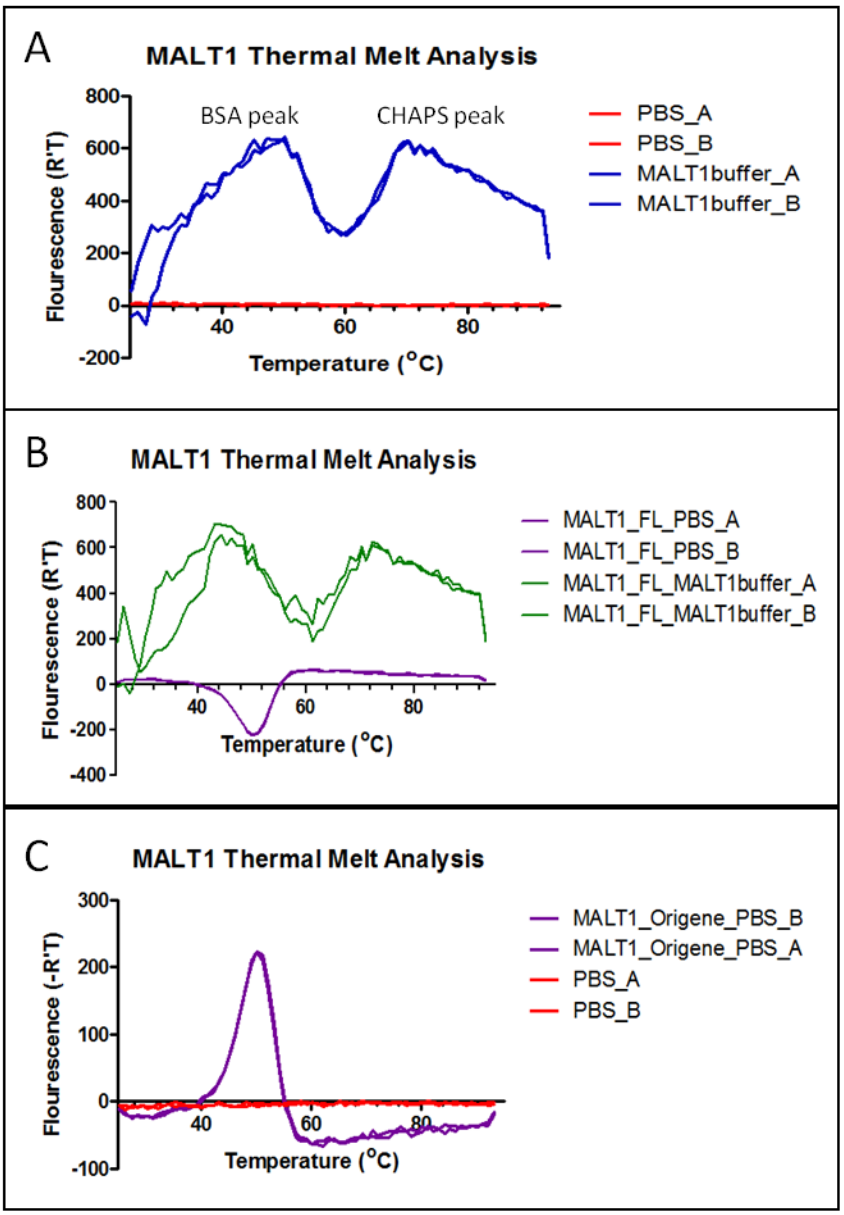
A
MALT1 Thermal Melt Analysis
BSA peak
CHAPS peak
Flourescence (R'T)
Temperature (°C)
PBS_A
PBS_B
MALT1buffer_A
MALT1buffer_B
B
MALT1 Thermal Melt Analysis
Flourescence (R'T)
Temperature (°C)
MALT1_FL_PBS_A
MALT1_FL_PBS_B
MALT1_FL_MALT1buffer_A
MALT1_FL_MALT1buffer_B
C
MALT1 Thermal Melt Analysis
Flourescence (-R'T)
Temperature (°C)
MALT1_Origene_PBS_B
MALT1_Origene_PBS_A
PBS_A
PBS_B

Figure 8. Optimization of MALT1 enzyme thermal melting curve. A) Derivative curve of the two buffers used, MALT1 biochemical assay buffer (blue) and PBS buffer (red) with SYPRO Orange dye without MALT1 protein [R'(t)]. The peaks associated with two buffer components, BSA and CHAPS, as determined in a different experiment. B) Dissociation curve of full length Origene MALT1 protein in MALT1 biochemical assay buffer (green) or PBS buffer (purple) [R'(t)]. C) Dissociation curve of full length Origene MALT1 protein in PBS buffer (purpe) or PBS buffer alone (red) [-R'(t)]. Each graph is a representative experiment of three experiments with similar results.

Thermal Shift of MALT1 with inhibitors

After optimization of the thermal melt assay conditions for MALT1, compounds known to bind MALT1 as well as novel MALT1 inhibitory compounds were examined in order to determine if the compounds bind MALT1 directly. First, each compound was analyzed for background fluorescence or interference with the fluorophore. Compounds were also analyzed at concentrations of 10 µM and 100 µM with MALT1 enzyme (Fig. 9). The effect of DMSO concentration on thermal melting was analyzed to ensure that any effect seen with the addition of compounds was not due to the DMSO present in the sample (Fig. 9A). A melting curve was observed for all DMSO conditions with MALT1 enzyme. The amplitude of the curve increased with an increasing concentration of DMSO, with the highest amplitude at 2.5% DMSO. The melting temperatures are 49.2°C for all experimental groups. DMSO concentration was kept constant at a final concentration of 1% in all samples, except the peptide inhibitor samples which contained 2.5% DMSO and the 2.5% DMSO control. When tested at 100 µM without enzyme, the fluorescence of mepazine remains flat upon temperature increase, indicating that the compound has no intrinsic fluorescence (Fig. 9B). The addition of 10 µM mepazine induces a large increase in amplitude and a slight increase in melting temperature from 49.2°C to 51.2°C. This may suggest compound binding to MALT1. The addition of 100 µM mepazine induces no increase in amplitude and no shift in melting temperature.

MI-2 was tested at 10 µM and 100 µM concentrations with and without MALT1 protein (Fig. 9C). The curve obtained when testing MI-2 at 100 µM without

protein is not flat, indicating that MI-2 has background fluorescence or some interference with the fluorophore. The melting temperature is 49.2°C for the DMSO control, 52.2°C for 10 µM MI-2, and unknown for 100 µM MI-2. The addition of 10 µM MI-2 induces an increase in amplitude and an increase in melting temperature. This may indicate compound binding to MALT1. The addition of 100 µM MI-2 induces a curve similar to the one seen without the addition of MALT1 enzyme. This may be because the compound is poorly soluble at 100 µM. Although there is some indication that MI-2 binds MALT1, collectively the data are difficult to interpret.

The peptide inhibitor, z-VRPR-Fmk, was tested at a concentration of 4 µM (Fig. 9D). The curve obtained with the peptide inhibitor at 4 µM without MALT1 protein is not perfectly flat, indicating that it has intrinsic fluorescence or some interference with the fluorophore. This background may not interfere with the assay, as a melting curve with the peptide and enzyme was observed. The melting temperature for MALT1 is 49.2°C at 2.5% DMSO and 49.2°C at 4 µM peptide. The addition of 2.5% DMSO induces an increase in peak amplitude and no shift in melting temperature. The addition of 4 µM z-VRPR-Fmk induces an increase in amplitude and no shift in melting temperature. This does not suggest compound binding to MALT1, although the higher DMSO concentration may interfere with MALT1's ability to bind compounds. A more concentrated sample of z-VRPR-Fmk should be tested in the future to investigate the binding event in order to allow for a lower concentration of DMSO in each test well.

The novel compounds A and B are small molecules that were discovered by Venenum Biodesign to inhibit MALT1 protease activity through a HTS utilizing the fluorescent peptide cleavage assay described in "MALT1 Fluorescence Assay". The compounds were tested at 10 µM and 100 µM concentrations (Fig. 9E and 9F). The melting temperatures for MALT1 with compound A are 49.2°C at 10 µM and 37.2°C at 100 µM. The melting temperatures for MALT1 with compound B are 50.2°C at 10 µM and 46.2°C at 100 µM. A left shift is observed at the 100 µM concentration for both compounds compared to DMSO control. Compound B exhibits background fluorescence when analyzed in the absence of MALT1 enzyme, however compound A does not.

An increase in melting temperature of MALT1 was seen with only mepazine or MI-2 at 10 µM. No shift was seen with any compound at 100 µM, or with the peptide inhibitor at 4 µM. Ambiguous results were seen with compounds A and B due to the small increase in temperature at 10 µM and large decrease in temperature at 100 µM. Further optimization of this assay is needed to confirm the possible thermal shift seen with 10 µM MI-2 or mepazine and elucidate MALT1 binding to compounds A and B.

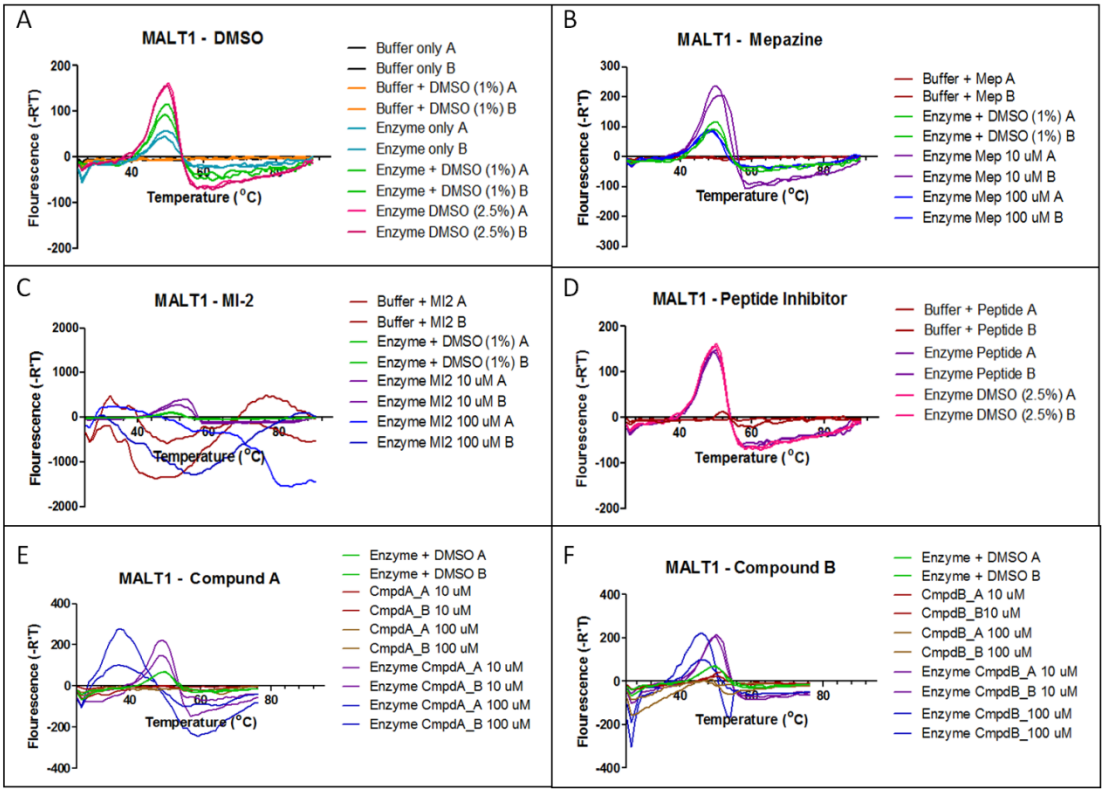
A
MALT1 - DMSO
Flourescence (-R'T')
Temperature (°C)
Buffer only A
Buffer only B
Buffer + DMSO (1%) A
Buffer + DMSO (1%) B
Enzyme only A
Enzyme only B
Enzyme + DMSO (1%) A
Enzyme + DMSO (1%) B
Enzyme DMSO (2.5%) A
Enzyme DMSO (2.5%) B
B
MALT1 - Mepazine
Buffer + Mep A
Buffer + Mep B
Enzyme + DMSO (1%) A
Enzyme + DMSO (1%) B
Enzyme Mep 10 uM A
Enzyme Mep 10 uM B
Enzyme Mep 100 uM A
Enzyme Mep 100 uM B
C
MALT1 - MI-2
Buffer + MI2 A
Buffer + MI2 B
Enzyme + DMSO (1%) A
Enzyme + DMSO (1%) B
Enzyme MI2 10 uM A
Enzyme MI2 10 uM B
Enzyme MI2 100 uM A
Enzyme MI2 100 uM B
D
MALT1 - Peptide Inhibitor
Buffer + Peptide A
Buffer + Peptide B
Enzyme Peptide A
Enzyme Peptide B
Enzyme DMSO (2.5%) A
Enzyme DMSO (2.5%) B
E
MALT1 - Compund A
Enzyme + DMSO A
Enzyme + DMSO B
CmpdA_A 10 uM
CmpdA_B 10 uM
CmpdA_A 100 uM
CmpdA_B 100 uM
Enzyme CmpdA_A 10 uM
Enzyme CmpdA_B 10 uM
Enzyme CmpdA_A 100 uM
Enzyme CmpdA_B 100 uM
F
MALT1 - Compound B
Enzyme + DMSO A
Enzyme + DMSO B
CmpdB_A 10 uM
CmpdB_B10 uM
CmpdB_A 100 uM
CmpdB_B 100 uM
Enzyme CmpdB_A 10 uM
Enzyme CmpdB_B 10 uM
Enzyme CmpdB_100 uM
Enzyme CmpdB_100 uM

Figure 9. Thermal shift of MALT1 enzyme and MALT1 inhibitors. All curves shown are dissociation curves [-R'(t)] plotted in GraphPad Prism. A) Melt curves of MALT1 enzyme with DMSO or without DMSO or DMSO and buffer without enzyme. B) Melt curves of MALT1 enzyme with DMSO or mepazine at 10 μM or 100 μM. 100 μM mepazine and buffer without MALT1 is shown as a red curve. C) Melt curves of MALT1 enzyme with DMSO or MI-2 at 10 μM or 100 μM. 100 μM MI-2 and buffer without MALT1 is shown as a red curve. D) Melt curves of MALT1 enzyme with 2.5% DMSO or 10 μM peptide inhibitor Z-VRPR-Fmk. 10 μM peptide inhibitor and buffer without MALT1 is shown as a red curve. E) Melt curves of MALT1 enzyme with DMSO or compound A at 10 μM or 100 μM. 100 μM mepazine and buffer without MALT1 is shown as a red curve. F) Melt curves of MALT1 enzyme with DMSO or compound B at 10 μM or 100 μM. 100 μM compound B and buffer without MALT1 is shown as a red curve. DMSO concentration was kept constant at a final concentration of 1% in each sample, unless indicated as in Figures 8A and 8D. Each graph is a representative experiment of three experiments with similar results.

Selection of Cell Lines for Proliferation and Protein Analysis Experiments

Investigation of protein expression in AML, DLBCL, and CLL cell lines is crucial for the understanding of pathway activation in the cell types as well as for confirmation of the presence of the target proteins MALT1 and BTK. Higher levels of NF-κB pathway activation may correlate with higher expression of MALT1, BTK, CYLD cleavage product (CYLD-CP), and RelB cleavage product (RelB-CP). CYLD and RelB are substrates of MALT1 that are cleaved when MALT1 is active. More cleavage of these proteins usually indicates a higher level of activation of MALT1. In order to determine protein expression, protein was extracted from cells and separated by gel electrophoresis. After transfer to a PVDF membrane, the membranes were probed for RelB, CYLD, MALT1, BTK, and GAPDH. Selected cell lines were the ABC-DLBCL cell lines OCI-LY-3 (Fig. 10A and 10B) and U-2932 (Fig. 10A), the GCB-DLBCL cell line SU-DHL-6 (Fig. 10A), the CLL cell line MEC-1 (Fig. 10A and 10B), and the AML cell lines OCI-AML-2 (Fig. 10B), OCI-AML-3 (Fig. 10B), and HL-60 (Fig. 10A).

Overall, MEC-1 has the highest expression of MALT1, CYLD full length (CYLD-FL), CYLD-CP, RelB full length (RelB-FL), and RelB-CP in comparison to the other cell lines. OCI-LY-3 and U-2932 cells have similar expression of MALT1 and CYLD, and U-2932 has slightly more RelB-FL than OCI-LY-3. MEC-1, SU-DHL-6, and U-2932 cells have similar expression of RelB-FL (Fig. 10A). RelB-CP was detected only in MEC-1 cells. CYLD-CP and CYLD-FL can be visualized faintly in Figure 10A with U-2932 and OCI-LY-3 cells, and more clearly with MEC-

1 cells. This cleavage product can be seen more clearly in Figure 10B with OCI-LY-3 and MEC-1 cells. Compared to OCI-LY-3 cells, where a similar amount of protein was loaded, HL-60 has low expression of all proteins relative to the GAPDH loading control, except BTK where a light band can be seen. BTK is highly expressed in the ABC-DLBCL and CLL cell lines, OCI-LY-3, U-2932, and MEC-1 (Fig. 10A). The GCB-DLBCL cell line, SU-DHL-6, has moderate expression of BTK. In all cell lines in Figure 10A, two BTK bands are present. The lower molecular weight protein may be a truncated isoform of BTK that is detectable when using a C-terminal or SH3-domain specific antibody [57]. In order to better understand the relationship between BTK and MALT1 and the effect of their inhibition on cell growth, cell lines were grouped by their relative expression of the two proteins. HL-60 was the only cell line that had higher BTK expression than MALT1. OCI-LY-3 was the only cell line that had relatively equal expression of the two proteins. MEC-1, SU-DHL-6, and U-2932 cells all had similar expression of both proteins, but slightly higher expression of MALT1 compared to BTK.

In a separate experiment, it was observed that OCI-AML-2 and OCI-AML-3 cells have similar expression of RelB-FL, RelB-CP, CYLD-FL, and CYLD-CP (Fig. 10B). Low expression of RelB-FL and RelB-CP, moderate expression of CYLD-FL, and no expression of CYLD-CP is seen in these AML cell lines. OCI-AML-2 has slightly higher expression of MALT1 than OCI-AML-3, but less than other cell lines. MEC-1 has high expression of all proteins that were probed for, which is consistent with the results seen in Figure 10A. OCI-LY-3 cells have moderate MALT1

expression, moderate expression of RelB-FL, and low expression of RelB-CP, CYLD-FL, and CYLD-CP. GAPDH was used as a loading control. Since expression of GAPDH is consistent between all samples in Figure 10B, loading of samples was even and changes in protein levels are not due to loading error. Low expression of GapDH in Figure 10A for HL-60 and OCI-LY-3 indicates that less protein was loaded onto the gel than for the other three cell lines. OCI-LY-3 cell protein expression in the two experiments was consistent even though less protein was loaded in Figure 10A. This suggests that even if a more concentrated lysate was examined, HL-60 cells would likely still have low expression of all proteins except BTK. This was corroborated by a later experiment (data not shown). All protein bands were compared to the protein standard to confirm length. The gel shown in Figure 10B was separated more than that shown in Figure 10A, making the cleavage product bands (CYLD-CP and RelB-CP) closer to the full length protein (CYLD-FL and RelB-FL) in Figure 10A than those in Figure 10B.

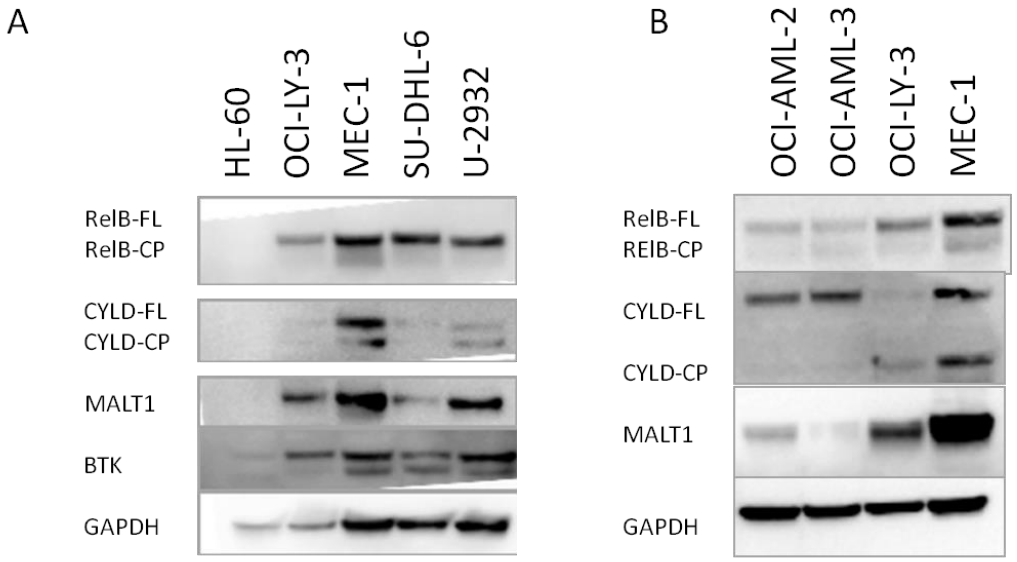

Figure 10. Protein expression of DLBCL, CLL, and AML cell lines. Western Blots showing expression of proteins within the NF-κB signaling pathway. A) HL-60, OCI-LY-3, MEC-1, SU-DHL-6, and U-2932 cell lysates were separated by gel electrophoresis and probed for RelB, CYLD, MALT1, BTK, and GapDH. B) OCI-AML-2, OCI-AML-3, OCI-LY-3, and MEC-1 cell lysates were separated by gel electrophoresis and probed for RelB, CYLD, MALT1, and GapDH. Each figure is a representative experiment of three experiments with similar results.

RelB Cleavage Assay

In order to monitor the cleavage of a MALT1 substrate and the effect of MALT1 inhibition on this cleavage, a western-based assay was developed. OCI-LY-3 cells were incubated with different experimental treatments, including 5 μM or 20 μM of MALT1 inhibitor Mepazine, DMSO, or the proteosome inhibitor MG-132. OCI-LY-3 cells have been shown to have robust activation of MALT1 and NF-κB signaling and thus high levels of RelB cleavage [3, 30, 32]. One would expect to see stabilization of the RelB cleavage product (RelB-CP) upon addition of the proteosome inhibitor MG-132, and a decrease in RelB-CP product upon the addition of a MALT1 inhibitor such as mepazine. Protein lysates were separated by gel electrophoresis and probed with Anti-RelB and Anti-GapDH antibodies (Fig. 11). An upper (RelB-FL) and lower band (RelB-CP) can be seen when probed for RelB at 70 and 55 kDa, respectively. A GapDH loading control verifies that the protein lysates were loaded in equal amounts. The untreated and DMSO lanes appear to have less RelB-FL than all other lanes, and little or no expression of RelB-CP. When treated with the proteosome inhibitor MG-132, with or without excess DMSO, RelB-CP appears faintly. This indicates that MG-132 is stabilizing the cleavage product. When Mepazine is added either at 5 μM or 20 μM with MG-132, a decrease in RelB-CP is not seen. There is, however, an increase in RelB-FL. This indicates that there may be a build-up of uncleaved RelB and therefore successful inhibition of MALT1.

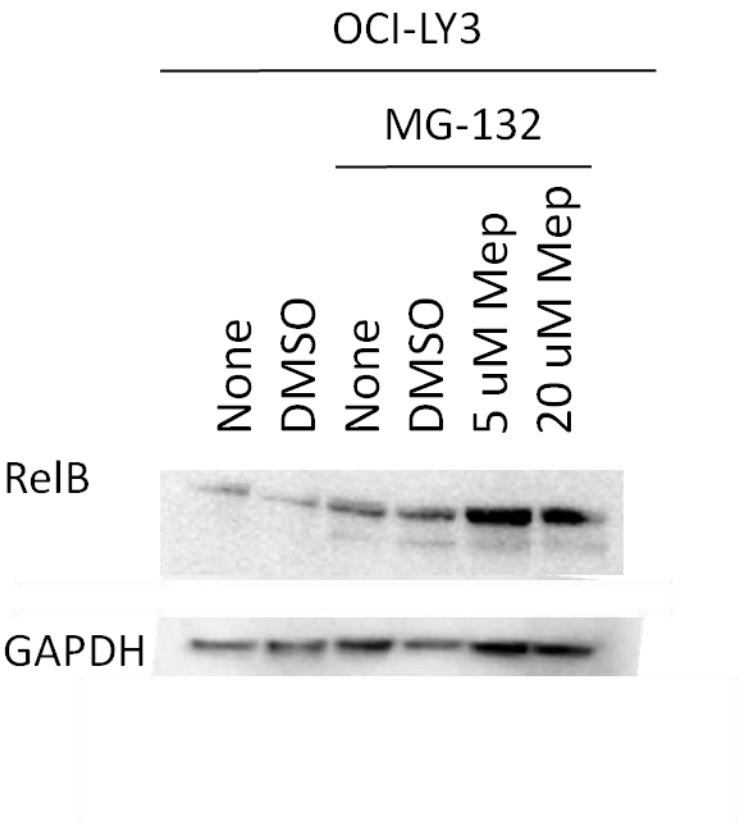

Figure 11. RelB cleavage in OCI-LY-3 cells. Levels of the MALT1 cleavage product RelB in OCI-LY-3 cells treated with combinations of MG-132, mepazine (Mep), or 1% DMSO control. DMSO concentration was kept constant at a final concentration of 1% in all samples. GAPDH loading control is included. This figure is a representative experiment of three experiments with similar results.

Cell Proliferation Optimization

In order to examine the effect of MALT1 or BTK inhibition on cell proliferation, an assay utilizing Promega's Cell Titer-Glo (CTG) system was developed. The assay first required optimization for ideal incubation time and ideal cell number for each cell line. Cells were seeded at densities ranging from 50,000 to 400 cells/well in a 384-well plate. The amount of ATP in each well was quantified by adding the CTG reagent and analyzing luminescence. Luminescence should correlate with ATP levels and reflects the number of viable cells. Figure 12 shows luminescence over time for each cell line, correlating with cell growth. The criteria for choosing ideal cell number was the lowest number of cells while maintaining at least a 2-fold increase in luminescence after the first 48 hours of incubation. This assay served to verify that cells were still in the logarithmic phase of growth at the endpoint of the assay before combining cells with inhibitory compounds. Ideal cell numbers were chosen to be: 6,000 cells/well for HL-60 and 1,500 cells/well for MEC1, OCI-AML-2, OCI-AML-3, and OCI-LY-3. These values are listed in Table 1. Cell doubling time was estimated using a line best fit to the chosen cell density. The estimated doubling time for each cell line is 25 hours for HL-60, 54 hours for OCI-AML-2, 20 hours for OCI-AML-3, 15 hours for OCI-LY-3, and 40 hours for MEC-1.

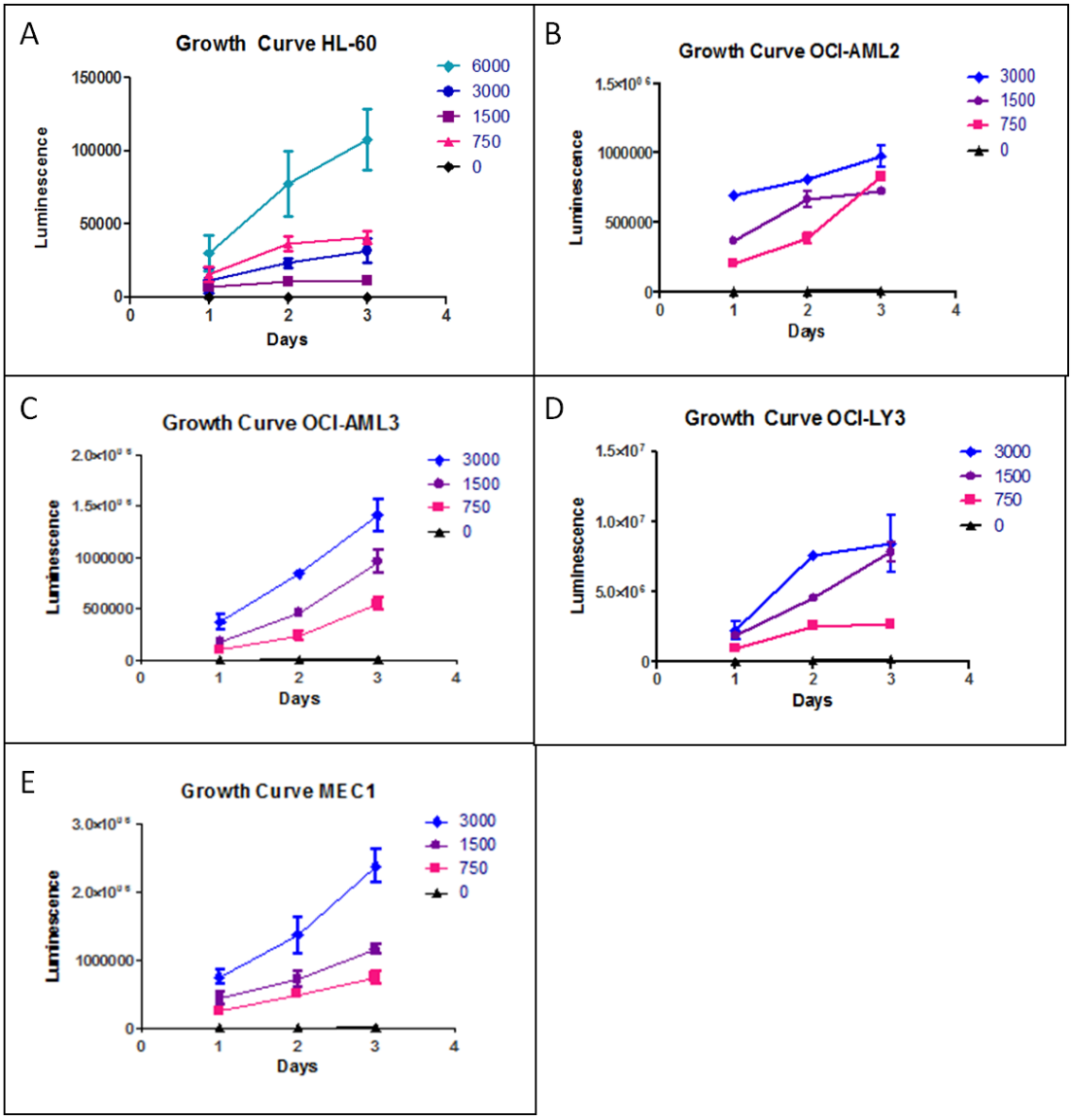
A
Growth Curve HL-60
Luminescence
Days
6000
3000
1500
750
0
B
Growth Curve OCI-AML2
Luminescence
Days
3000
1500
750
0
C
Growth Curve OCI-AML3
Luminescence
Days
3000
1500
750
0
D
Growth Curve OCI-LY3
Luminescence
Days
3000
1500
750
0
E
Growth Curve MEC1
Luminescence
Days
3000
1500
750
0

Figure 12. Cell proliferation titration and optimization. Luminescence of cell titrations of different cell lines over three or four days, acquired using CellTiter-Glo reagent. Day 0 indicates time of seeding. Readings were taken at 24 hour increments following seeding. Concentrations ranging from 750 – 6,000 cells input per well are shown for each cell line, including the AML cell lines HL-60 (Fig. 11A), OCI-AML-2 (Fig. 11B), OCI-AML-3 (Fig. 11C), the DLBCL cell line OCI-LY-3 (Fig. 11D), and the CLL cell line MEC-1 (Fig. 11E). Each graph is a representative experiment of three experiments with similar results.

Cell Proliferation with Single Agent Compounds

Once the ideal cell number was chosen for the proliferation assay, compound serial dilutions were added to different cell lines in order to analyze their effect on the proliferation of different cell types. The MALT1 inhibitors mepazine and MI-2 as well as the BTK inhibitor Ibrutinib were chosen for examination. Cells with and without compounds were analyzed for ATP levels using CTG after incubation for 2 days. Luminescence was plotted versus the logarithm of inhibitor molarity (log(M)) (Fig. 13). Curve bottom, curve top, IC_{50}, and Hill slope are listed below each graph.

Figure 13A shows the dose response curves for the AML cell line HL-60, with mepazine, MI-2, or Ibrutinib. All HL-60 curves show dose-dependent inhibition. The IC_{50} values are 29 µM, 0.17 µM, and 32 µM for mepazine, MI-2, and Ibrutinib, respectively. The dose response curves for all of the three compounds are sigmoidal in shape. There is an obvious shift to the left when comparing MI-2 to mepazine or Ibrutinib, indicating that MI-2 is more effective at inhibiting growth in the specific cell line. Figure 13B shows the dose response curves for the AML cell line OCI-AML-3 with the compounds mepazine or MI-2. The IC_{50} values are 24 µM and 1.5 µM for mepazine and MI-2, respectively, suggesting that MI-2 has better potency than mepazine.

Figure 13C shows the dose response curves for the ABC-DLBCL cell line OCI-LY-3 with mepazine or Ibrutinib. The IC_{50} values are 23 µM and 8.4 µM for mepazine and Ibrutinib, respectively. This indicates that Ibrutinib is more effective at inhibiting OCI-LY-3 cell growth than is Mepazine. Figure 13D shows the dose

response curves for the CLL cell line, MEC-1, with mepazine or Ibrutinib. The two compounds inhibit MEC-1 cell growth with similar potency and efficacy. The IC_{50} values are 18 μM and 12.9 μM for mepazine and Ibrutinib, respectively. Figure 13E shows the dose response curves for the GCB-DLBCL cell line, SU-DHL-6, with mepazine or Ibrutinib. The IC_{50} values are 16 μM and 1 μM for mepazine and Ibrutinib, respectively. There is a shift along the x-axis between compounds, indicating that Ibrutinib more effectively inhibits growth of SU-DHL-6 cells than does mepazine.

There is a trend among the AML cell lines HL-60 and OCI-AML-3. The IC_{50} values for the mepazine curves are very similar for both cell lines, differing by only 20%. In both experiments, MI-2 is more potent than mepazine by at least 10-fold. The HL-60 cell line is the most sensitive to MALT1 inhibition compared to other cell lines, but resistant to BTK inhibition. In all other cell lines, including OCI-LY-3, MEC-1, and SU-DHL-6, results suggest that Ibrutinib is more effective at slowing the proliferation of the various cells, but the results are difficult to interpret. Ibrutinib has the highest efficacy when examined with the GCB-DLBCL cell line, SU-DHL-6 compared to the other cell lines, suggesting that this cell line is most sensitive to BTK inhibition. No correlation was observed between doubling time of the cells and sensitivity to MALT1 or BTK inhibition.

A

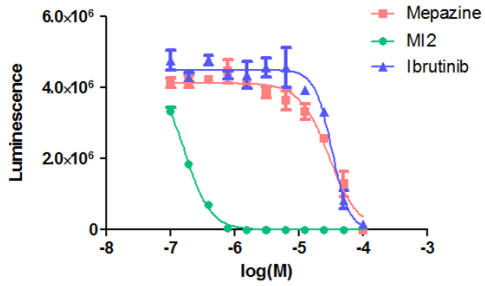

	MI2	Mepazine	Ibrutinib
Bottom	= 0.0	= 0.0	= 0.0
Top	4.394e+006	4.118e+006	4.488e+006
LogIC50	-6.772	-4.528	-4.484
HillSlope	-2.145	-1.915	-3.228
IC50	1.691e-007	2.965e-005	3.278e-005
Span	= 4.394e+006	= 4.118e+006	= 4.488e+006

B

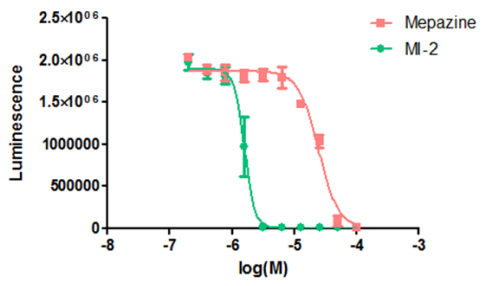

	MI-2	Mepazine
Bottom	= 0.0	= 0.0
Top	1.895e+006	1.867e+006
LogIC50	-5.803	-4.614
HillSlope	-5.264	-2.716
IC50	1.573e-006	2.435e-005
Span	= 1.895e+006	= 1.867e+006

C

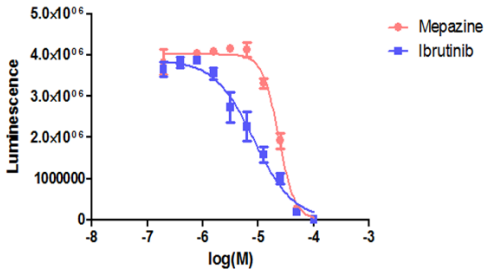

	Mepazine	Ibrutinib
Best-fit values		
Bottom	= 0.0	= 0.0
Top	4.007e+006	3.864e+006
LogIC50	-4.630	-5.074
HillSlope	-2.979	-1.226
IC50	2.346e-005	8.434e-006
Span	= 4.007e+006	= 3.864e+006

D

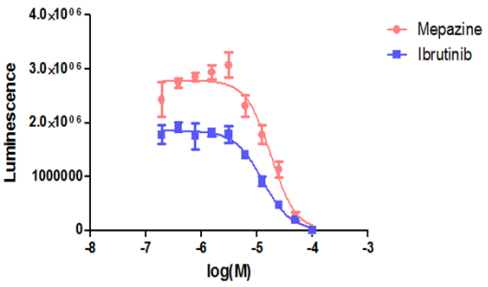

	Mepazine	Ibrutinib
Bottom	= 0.0	= 0.0
Top	2.784e+006	1.851e+006
LogIC50	-4.740	-4.888
HillSlope	-1.954	-1.721
IC50	1.820e-005	1.294e-005
Span	= 2.784e+006	= 1.851e+006

E

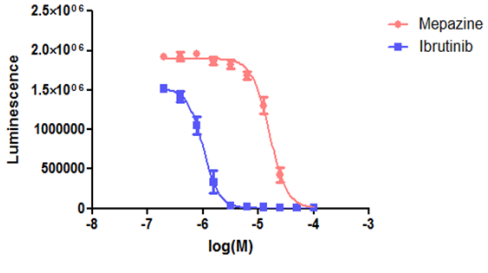

	Mepazine	Ibrutinib
Best-fit values		
Bottom	= 0.0	= 0.0
Top	1.894e+006	1.517e+006
LogIC50	-4.795	-5.991
HillSlope	-2.757	-2.976
IC50	1.602e-005	1.021e-006
Span	= 1.894e+006	= 1.517e+006

Figure 13. Cell viability of CLL, AML, and DLBCL cells treated with MALT1 (Mepazine or MI-2) or BTK inhibitors (Ibrutinib). Cells were incubated with inhibitors for 72 hours after seeding and luminescence was read using the CTG reagent (Promega). Dose response curves are shown as Luminescence v. log(M) with four parameter analysis conditions listed below each graph. A) Dose response curves for the AML cell line, HL-60, when treated with mepazine, MI-2, or Ibrutinib. B) Dose response curves for the AML cell line, OCI-AML-3, when treated with mepazine or MI-2. C) Dose response curves for the ABC-DLBCL cell line, OCI-LY-3, when treated with mepazine or Ibrutinib. D) Dose response curves for the CLL cell line, MEC-1, when treated with mepazine or Ibrutinib. E) Dose response curves for the GCB-DLBCL cell line, SU-DHL-6, when treated with mepazine or Ibrutinib. Each graph is a representative experiment of three experiments with similar results.

Combinatorial Cell Proliferation Assay

In order to investigate synergy between the BTK inhibitor Ibrutinib and the MALT1 inhibitor mepazine, a combinatorial study was developed. The assay is similar to the proliferation assay described previously, monitoring ATP with CTG reagent. Cell lines were selected based on their sensitivity to MALT1 or BTK inhibition in the single agent experiment "Cell Proliferation with Single Agent Compounds" and their protein expression in "Selection of Cell Lines". BTK inhibitor sensitive (SU-DHL-6) and resistant (OCI-LY-3) cell lines were chosen in order to determine if the addition of mepazine improved the response of the resistant cells to treatment. A matrix layout was utilized in order to test 6 different concentrations of each compound, for a total of 49 combinations. Analysis was performed using the highest single agent and Bliss additivism models, as described in A.A. Borisy, et al., 2003 [56]. Crucial steps in the analysis are shown, such as calculation of the percent inhibition from raw luminescence values and calculation of the predicted response using the highest single agent and Bliss additivism methods (Fig. 14). Results using the ABC-DLBCL cell line, OCI-LY-3 are shown in Figures 15A and 15B, and the GCB-DLBCL cell line, SU-DHL-6 are shown in Figures 15C and 15D. All concentrations are given in μM. A dilution of Ibrutinib is shown in the rows, and a dilution of mepazine is shown in the columns. Values in the matrix are given as percent inhibition in excess of the predicted value, estimated by either the highest single agent method (Fig. 14A and 14C) or Bliss additivism (Fig. 15B or 15D).

Higher percent excess over the predicted value tended to appear in the center of the matrix as opposed to the extreme high or low concentration values. The highest percent excess that is seen while using the OCI-LY-3 cells is with 11 µM mepazine and 11 µM Ibrutinib (Fig. 15A and 15B). The predicted reaction was 34% inhibition by the highest single agent method and 49% by Bliss additivism. The observed reaction was 65%, which was 31% over the highest single agent and 16% over the bliss additivism model. The highest observed excess that is seen while using the SU-DHL-6 cells differs between different methods of analysis. The combination of 11 µM Mepazine and either 1.2 µM or 0.4 µM Ibrutinib show the highest percent excess over the highest single agent. These values are 21% and 25% for 1.2 µM Ibrutinib or 0.4 µM Ibrutinib, respectively. Similarly, 21% excess over the highest single agent can be seen with 3.7 µM mepazine and 0.4 µM Ibrutinib. This differs slightly from the result using the Bliss additivism model. The highest values seen were using 11 µM or 3.7 µM mepazine and 1.2 µM Ibrutinib. The percent excess is much less than was seen with the highest single agent analysis. These values are 6.8% and 7.2% for 11 µM and 3.7 µM mepazine, respectively.

In order to better examine the ability of mepazine to increase the effectiveness of Ibrutinib, dose response curves for Ibrutinib alone and with 11 µM mepazine were plotted (Fig. 16). The effect on OCI-LY-3 (Fig. 16A) and SU-DHL-6 (Fig. 16B) cells is shown. Both cell lines displayed an increase in Ibrutinib potency with the addition of 11 µM mepazine. When mepazine is added, a decrease in IC_{50} is observed from 21

μM to 7 μM (3-fold shift) and from 530 nM to 98 nM (5-fold shift) for OCI-LY-3 and SU-DHL-6 cells, respectively.

A

Ibrutinib (μM) \ Mepazine (μM)	100.0	33.3	11.1	3.7	1.2	0.4	0.0
100.0	149500	6800	8600	9400	9000	10300	13600
33.3	148600	82200	167300	273300	282300	322500	343100
11.1	181800	234200	405500	673000	701300	752300	764200
3.7	199200	352900	701600	921600	892200	870000	942300
1.2	207800	402200	701600	847400	863500	969900	1007800
0.4	161900	405600	816000	883600	924100	942300	1099800
0.0	216300	452100	888900	893100	1031700	1028800	1158600

B

Ibrutinib (μM) \ Mepazine (μM)	100.0	33.3	11.1	3.7	1.2	0.4	0.0
100.0	0.871	0.994	0.993	0.992	0.992	0.991	0.988
33.3	0.872	0.929	0.856	0.764	0.756	0.722	0.704
11.1	0.843	0.798	0.650	0.419	0.395	0.351	0.340
3.7	0.828	0.695	0.394	0.205	0.230	0.249	0.187
1.2	0.821	0.653	0.394	0.269	0.255	0.163	0.130
0.4	0.860	0.650	0.296	0.237	0.202	0.187	0.051
0.0	0.813	0.610	0.233	0.229	0.110	0.112	0.000

C

Ibrutinib (μM) \ Mepazine (μM)	100.0	33.3	11.1	3.7	1.2	0.4	0.0
100.0	0.988	0.988	0.988	0.988	0.988	0.988	0.988
33.3	0.813	0.704	0.704	0.704	0.704	0.704	0.704
11.1	0.813	0.610	0.340	0.340	0.340	0.340	0.340
3.7	0.813	0.610	0.233	0.229	0.187	0.187	0.187
1.2	0.813	0.610	0.233	0.229	0.130	0.130	0.130
0.4	0.813	0.610	0.233	0.229	0.110	0.112	0.051
0.0	0.813	0.610	0.233	0.229	0.110	0.112	0.000

D

Ibrutinib (μM) \ Mepazine (μM)	100.0	33.3	11.1	3.7	1.2	0.4	0.0
100.0	0.998	0.995	0.991	0.991	0.990	0.990	0.988
33.3	0.945	0.884	0.773	0.772	0.736	0.737	0.704
11.1	0.877	0.743	0.494	0.492	0.413	0.414	0.340
3.7	0.848	0.683	0.376	0.373	0.276	0.278	0.187
1.2	0.838	0.661	0.333	0.329	0.225	0.228	0.130
0.4	0.823	0.630	0.272	0.268	0.155	0.157	0.051
0.0	0.813	0.610	0.233	0.229	0.110	0.112	0.000

Figure 14. Representative matrix calculation for highest single agent and Bliss additivism predicted response values. A) Average raw luminescence values for OCI-LY-3 dose response matrix. B) Calculated fractional inhibition for each point in the matrix based on DMSO control well luminescence, where 0 is no inhibition and 1.0 is complete inhibition. C) Predicted response of percent inhibition based on the highest single agent method. D) Predicted response of percent inhibition based on the Bliss additivism method. Dose matrixes are color-coded where red is the highest value and green is the lowest value.

A

Mepazine (μM)

Ibrutinib (μM)	100.0	33.3	11.1	3.7	1.2	0.4	0.0
100.0	*-11.7*	0.6	0.4	0.4	0.4	0.3	*0.0*
33.3	5.8	22.5	15.2	6.0	5.2	1.8	*0.0*
11.1	3.0	18.8	31.0	7.9	5.4	1.0	*0.0*
3.7	1.5	8.6	16.2	*-2.5*	4.3	6.2	*0.0*
1.2	0.7	4.3	16.2	3.9	12.5	3.3	*0.0*
0.4	4.7	4.0	6.3	0.8	9.3	7.5	*0.0*
0.0	*0.0*	*0.0*	*0.0*	*0.0*	*0.0*	*0.0*	*0.0*

% excess over Highest Single Agent

B

Mepazine (μM)

Ibrutinib (μM)	100.0	33.3	11.1	3.7	1.2	0.4	0.0
100.0	*-12.7*	*-0.1*	0.2	0.1	0.3	0.2	*0.0*
33.3	*-7.3*	4.5	8.3	*-0.8*	2.0	*-1.5*	*0.0*
11.1	*-3.4*	5.5	15.6	*-7.2*	*-1.8*	*-6.4*	*0.0*
3.7	*-2.0*	1.3	1.8	*-16.9*	*-4.6*	*-2.9*	*0.0*
1.2	*-1.7*	*-0.8*	6.2	*-6.1*	2.9	*-6.5*	*0.0*
0.4	3.7	2.0	2.4	*-3.1*	4.8	3.0	*0.0*
0.0	*0.0*	*0.0*	*0.0*	*0.0*	*0.0*	*0.0*	*0.0*

% excess over Bliss additivism

C

Mepazine (μM)

Ibrutinib (μM)	100.0	33.3	11.1	3.7	1.2	0.4	0
100.0	*-11.1*	0.3	0.3	0.3	0.2	0.2	*0.0*
33.3	*-10.1*	0.3	0.5	0.4	0.3	0.3	*0.0*
11.1	*-9.8*	0.8	0.5	0.2	0.5	0.2	*0.0*
3.7	*-6.5*	3.5	3.1	2.7	2.3	1.3	0.0
1.2	5.5	11.8	20.9	15.1	8.7	6.4	*0.0*
0.4	5.1	8.7	25.0	20.8	15.9	5.8	*0.0*
0	*0.0*	*0.0*	*0.0*	*0.0*	*0.0*	*0.0*	*0.0*

% excess over Highest Single Agent

D

Mepazine (μM)

Ibrutinib (μM)	100.0	33.3	11.1	3.7	1.2	0.4	0
100.0	*-11.8*	*-0.4*	*-0.2*	0.0	*0.0*	0.1	*0.0*
33.3	*-10.5*	*-0.2*	0.1	0.2	0.2	0.3	*0.0*
11.1	*-10.7*	*-0.1*	*-0.1*	*-0.1*	0.2	0.2	*0.0*
3.7	*-9.7*	0.0	0.8	1.4	1.4	1.1	*0.0*
1.2	*-9.1*	2.4	6.9	7.2	3.2	5.0	*0.0*
0.4	*-4.2*	2.7	5.2	3.5	4.0	2.9	*0.0*
0	*0.0*	*0.0*	*0.0*	*0.0*	*0.0*	*0.0*	*0.0*

% excess over Bliss additivism

Figure 15. Combinatorial proliferation assay with BTK inhibitor Ibrutinib and MALT1 inhibitor mepazine. OCI-LY-3 (Fig. 14A and 14B) or SU-DHL-6 (Fig. 14C and 14D) cells with a dose matrix consisting of six concentrations each of Ibrutinib (rows) and mepazine (columns), with a total of 49 combinations. Data was analyzed using the highest single agent (Fig. 14A and 14C) or Bliss additivism (Fig. 14B and 14D) method and is shown as percent excess over the predicted value. Red highlighted cells indicate the highest percent excess over the predicted value and yellow values indicate a percent excess that is closer to zero. Values less than or equal to zero are uncolored. Each graph is a representative experiment of three experiments with similar results.

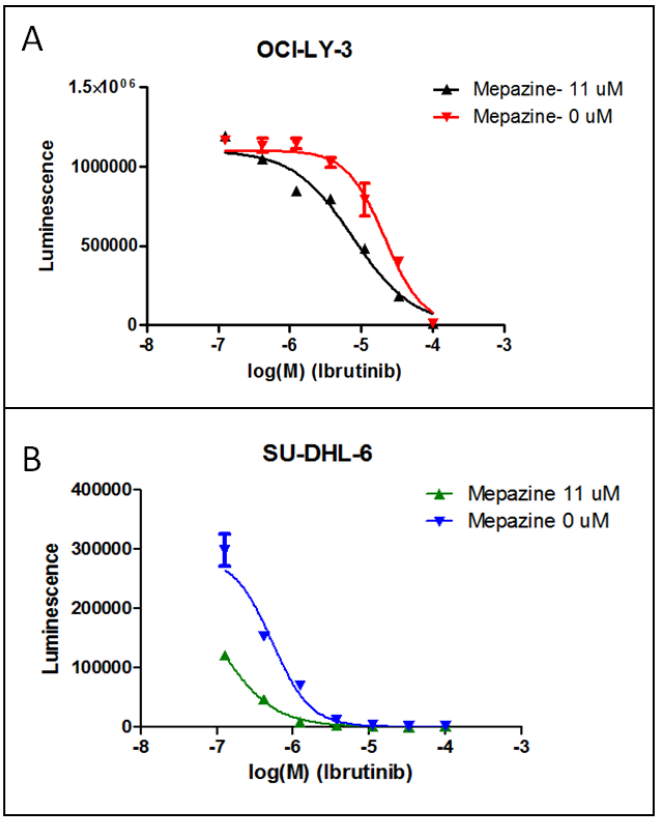

C

	OCI-LY-3		SU-DHL-6	
	Mepazine- 11 uM	Mepazine- 0 uM	Mepazine- 11 uM	Mepazine- 0 uM
Bottom	= 0.0	= 0.0	= 0.0	= 0.0
Top	= 1.100e+006	= 1.100e+006	= 287600	= 287600
LogIC50	-5.111	-4.673	-7.009	-6.277
HillSlope	-1.035	-1.626	-1.203	-1.715
IC50	7.75E-06	2.13E-05	9.79E-08	5.29E-07
R square	0.928	0.982	0.993	0.968

Figure 16. Effectiveness of Ibrutinib is increased with the addition of 11 µM mepazine in DLBCL cell lines. A) OCI-LY-3 cells treated with a serial dilution of Ibrutinib with or without 11 µM mepazine. B) SU-DHL-6 cells treated with a serial dilution of Ibrutinib with or without 11 µM mepazine. C) Span, IC_{50}, R square, and Hill slope values for each experimental condition.

Summary of Experiments

A summary table of all pIC_{50} values and standard deviation (SD) was created to better examine consistency between experiments (Fig. 17) and compare experimental values to published pIC_{50} values. Figure 16A shows pIC_{50} values and standard deviation (SD) from the fluorescent peptide cleavage assay (Fig. 6) and published IC_{50} values [2-4]. With the exception of three compounds all SD are below 0.3, indicating that the compounds reliably inhibited MALT1 over multiple experiments. Included in this list of reliable inhibitors are mepazine, MI-2, z-VRPR-Fmk, and β-Lapachone. Thioridazine, compound A, and compound B had large differences in pIC_{50} values between experiments, which indicates that the compounds did not perform accurately and reproducibly over multiple experiments.

Figure 16B shows pIC_{50} values and standard deviation (SD) from the cell proliferation assay with single agent compounds (Fig. 12). All experiments performed more than once had SD values that were less than 0.3, with the exception of one experiment (MEC-1 treated with Ibrutinib). This experiment was only performed twice and should be repeated in the future to ensure a more accurate pIC_{50}. A SD below 0.3 indicates that a consistent response to the inhibitor was seen in the cells over multiple experiments.

A

Biochemical Assay pIC_{50} and Standard Deviation (SD)

	N=1	N=2	N=3	N=4	N=5	Average pIC_{50}	SD	Published pIC50
Mepazine	6.14	6.43	6.43	6.29	6.20	6.30	0.13	6.08
MI-2	6.19	6.17	6.64			6.34	0.26	5.23
z-VRPR-Fmk	9.91	9.55	9.34			9.60	0.29	
Thioridazine	5.29	3.60				4.45	1.19	5.46
β-Lapachone	5.39	5.23				5.31	0.11	5.72
Compound A	5.21	5.37	5.31			5.30	0.04	
Compound B	5.21	5.25	5.35			5.27	0.07	

B

Cell Proliferation Assay pIC_{50} and Standard Deviation (SD)

HL-60	**N=1**	**N=2**	**N=3**	**N=4**	**N=5**	**Average pIC_{50}**	**SD**
Mepazine	-4.528	-4.599	-5.049	-4.529	-4.678	-4.677	0.217
MI-2	-6.772					-6.772	
Ibrutinib	-4.484	-4.539	-5.085	-4.622	-4.468	-4.640	0.256
MEC-1							
Mepazine	-4.377	-4.740				-4.559	0.257
MI-2	-6.246	-6.157				-6.202	0.063
Ibrutinib	-4.888	-4.261				-4.575	0.443
OCI-AML-3							
Mepazine	-4.614					-4.614	
MI-2	-5.803					-5.803	
OCI-LY-3							
Mepazine	-4.562	-4.581	-4.630	-4.999		-4.693	0.206
Ibrutinib	-4.686	-4.976	-5.074	-5.229	-4.616	-4.916	0.260
SU-DHL-6							
Mepazine	-5.056	-4.795	-4.795	-4.602		-4.812	0.186
Ibrutinib	-6.310	-6.027	-5.991			-6.109	0.175

Figure 17. Summary pIC_{50} and standard deviation tables. A) pIC_{50} values and standard deviation of all experiments performed with the MALT1 inhibitors mepazine, MI-2, z-VRPR-Fmk, thioridazine, β-Lapachone, and the novel compounds A and B in a biochemical fluorescent peptide cleavage assay. Published pIC_{50} values are shown [2-4]. B) pIC_{50} values and standard deviation of all experiments performed with the MALT1 inhibitors mepazine and MI-2, and the BTK inhibitor Ibrutinib in a cell based proliferation assay that monitored ATP.

Transfection Optimization

Transfection of siRNA and plasmid DNA into cells could be useful for future experiments. MALT1 or BTK siRNA could be used to examine the effect of MALT1 or BTK knockdown on pathway activation and cell proliferation of different cell types. This could elucidate the role of those proteins in tumor cell survival. SiRNA knockdown cells could be compared to cells treated with small molecule inhibitors and degree of inhibition characterized. Cell transfected with plasmid DNA, such as an NF-κB reporter plasmid, could be used to analyze the effect of MALT1 or BTK inhibition on NF-κB activity directly. MEC-1 cells were chosen for transfection because of the cells' robust activation of NF-κB that was shown by western, sensitivity to MALT1 or BTK inhibition, and accessibility to successful transfection protocols.

In order introduce siRNA or plasmid DNA into difficult-to-transfect MEC-1 cells, cells were subjected to electroporation. SiGLO siRNA and a GFP plasmid construct were utilized to examine the efficacy of nucleofection of cells with various conditions and for subsequent protocol optimization. Figure 18A shows the forward and side scatter of the mock transfected cell population 24 hours after transfection. The population was gated by size to distinguish live and dead cells. 60% of the population is dead and 35.7% of the population is alive upon analysis. Future populations in this experiment were gated using these conditions. Figure 18B shows a histogram of GFP emission of siGLO siRNA transfected cells and mock transfected population at different time points after transfection. The blue curve represents a

population of cells after 24 hours and the green curve represents a population of cells after 48 hours. There is a right shift along the x-axis when comparing transfected and mock transfected cell populations. This represents the presence of more cells with GFP emission, and thus siGLO siRNA inside the cell.

Similarly, Figure 18C shows a histogram of GFP emission of plasmid DNA transfected cells and mock transfected cells at different time points after transfection. The blue curve represents a population of cells after 24 hours and the green curve represents a population of cells after 48 hours. Less of a right shift can be seen with the GFP plasmid transfected cell populations compared to the siRNA transfection, but a small amount of varied GFP expressing cells can be seen. Although a shift in GFP production is not obvious, it seems that the cells may be producing varied amounts of GFP, suggesting that the transfection was successful to some extent. Selection and expansion of a single clone would allow for the creation of a cell line stably maintaining the transfected DNA and subsequent analysis of MALT1 inhibition directly on NF-κB activity. In the future, this transfection protocol could be used to introduce siRNA or plasmid DNA into MEC-1 cells or other similar difficult-to-transfect cells.

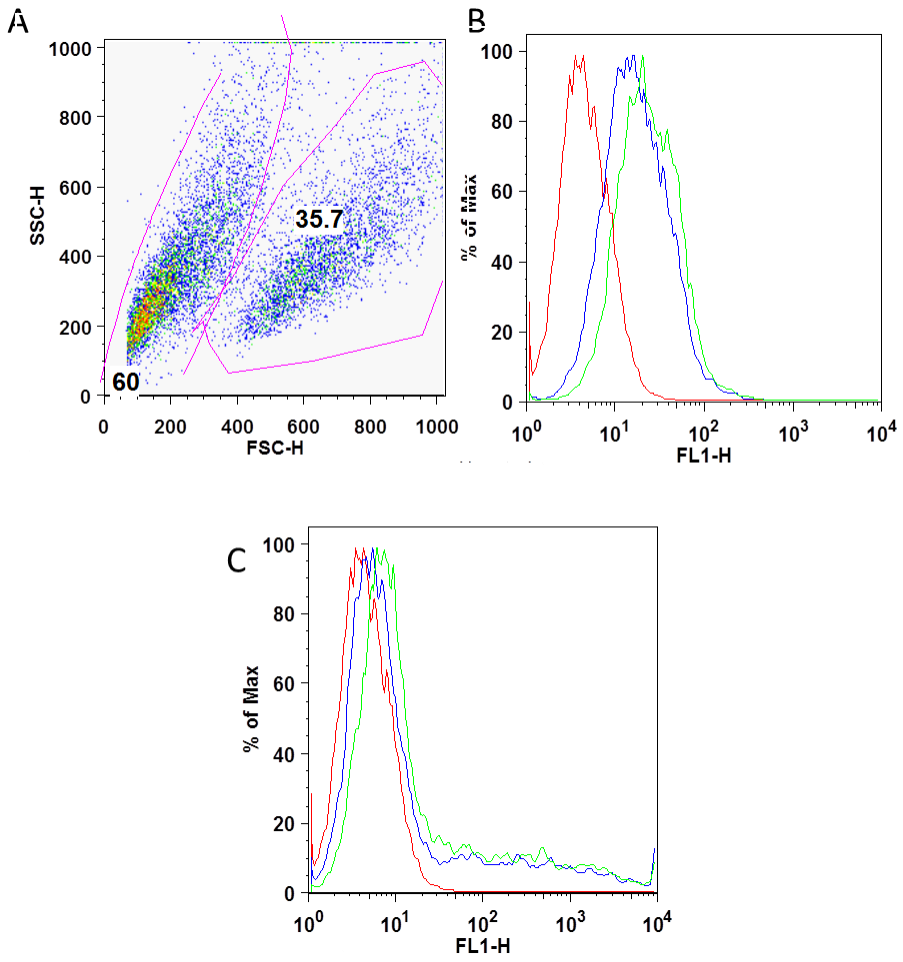

Figure 18. Flow cytometry analysis of transfection efficacy using siGLO siRNA or pGFP plasmid DNA and MEC-1 cells. A) Gating of live (35.7%, right) v. dead (60%, left) mock transfected cells. B) Un-gated siGLO transfected cells at 24 hours (blue) or 48 hours (green) and mock transfected cells (red). C) Un-gated pGFP transfected cells at 24 hours (blue) or 48 hours (green) and mock transfected cells (red). Each graph is a representative experiment of three experiments with similar results.

Figure 19A and 19B show a histogram of GFP expression for GFP plasmid transfected cells 48 hours post-transfection. Each graph shows gated populations of live (Fig. 19A) or dead (Fig. 19B) cells. The blue curve represents GFP transfected cells and the red curve represents mock transfected cells. There is a right shift along the x-axis that can be seen when comparing the live GFP transfected cells to the mock transfected cells (Fig. 19A). There is a peak of low-level GFP expressing cells and a larger amount of higher-level GFP expressing cells, seen as many lower peaks to the right of the main peak. There is no obvious right shift when comparing dead GFP transfected cells to mock transfected cells (Fig. 19B). Upon analysis of the live cell population, it was determined that 67% are GFP +, while only 4% of the dead cells are GFP +. This indicates that the majority of cells expressing GFP plasmid survived the transfection with the ability to produce GFP protein.

Figure 19C and 19D show a histogram of siGLO transfected cells 24 hours post-transfection. Each graph shows gated populations of live (Fig. 19C) or dead (Fig. 19D) cells. The blue curve represents GFP transfected cells and the red curve represents mock transfected cells. There is a right shift that can be seen when comparing both live and dead siGLO transfected cells to mock transfected cells. There is a more significant shift that can be seen when examining the dying siGLO transfected cells than with the live cells. Only 12% of the live cell population is siGLO +, whereas 51% of the dead cell population is siGLO +. This indicates that the cells either did not survive the transfection, or the siGLO reagent prohibits cell growth and survival once inside the cell.

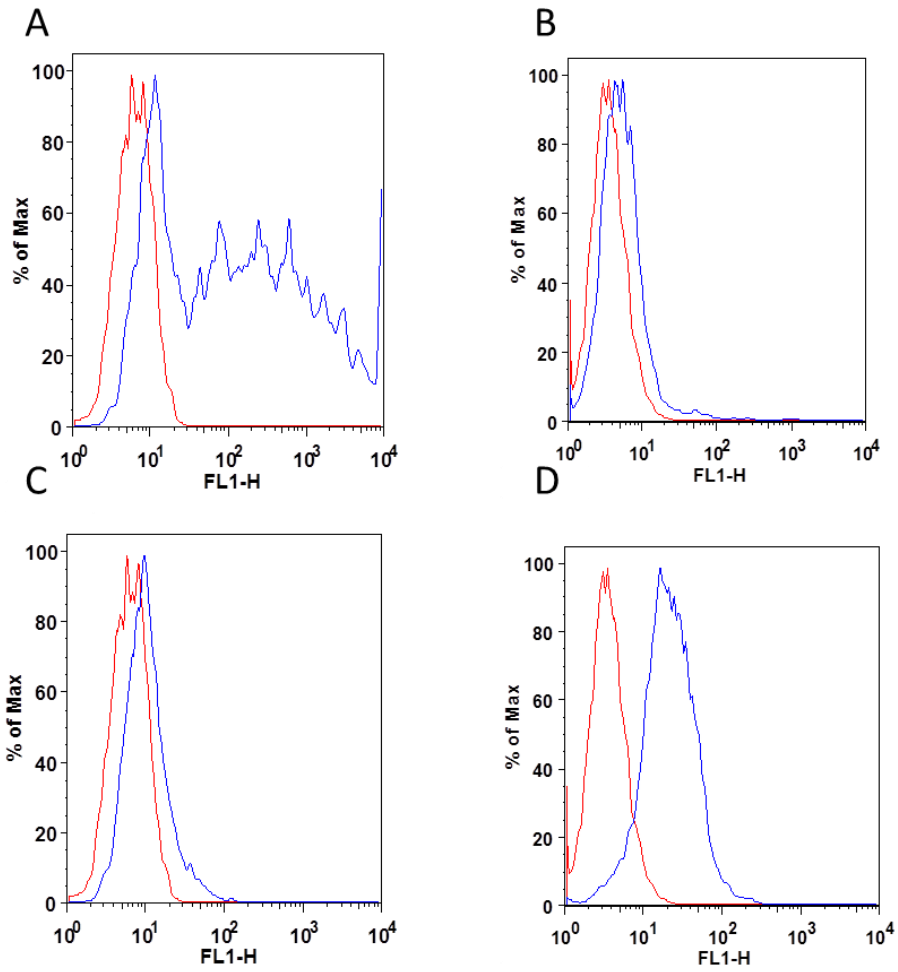

Figure 19. Analysis of transfected MEC-1 cell viability and efficacy of transfection. A) Gated population of live GFP plasmid transfected MEC1 cells at 48 hours (blue) and mock transfected cells (red) are shown (67% GFP +). B) Gated population of dead GFP plasmid transfected MEC1 cells at 48 hours (blue) and mock transfected cells (red) are shown (4% GFP +). C) Gated population of live siGLO transfected MEC1 cells at 24 hours (blue) and mock transfected cells (red) are shown (12% siGLO +). D) Gated population of dead siGLO transfected MEC1 cells at 24 hours (blue) and mock transfected cells (red) are shown (51% siGLO +). Each graph is a representative experiment of three experiments with similar results.

Discussion

Biochemical Characterization of MALT1 inhibitors

Inhibition of MALT1 could be effective at slowing the growth of different types of leukemia and lymphoma, especially types that are dependent on BCR or NF-κB signaling. Multiple inhibitors for MALT1 exist, but have never been characterized together in a single assay. In order to examine compound effectiveness, a fluorescent peptide cleavage assay was used. The assay will provide information that is crucial for analysis of novel compound mechanism of action and efficacy compared to known inhibitors.

Seven single agent compound dilutions were analyzed, mepazine, MI-2, a peptide inhibitor (z-VRPR-Fmk), thioridazine, β-Lapachone, and two novel compounds (A and B) discovered at Venenum Biodesign. Dose dependent inhibition of MALT1 could be seen with all compounds. The most striking result that can be drawn from these data is the high potency of the peptide inhibitor compared to the other inhibitors. The IC_{50} value is in the sub-nanomolar range, whereas the other compounds are in the micromolar range. This indicates that z-VRPR-Fmk is able to inhibit 50% of the enzyme present with as low a concentration as 0.35 nM. A much higher concentration of compound is necessary to obtain the same level of inhibition with the other four compounds (0.5 μM- 7 μM). Since the peptide inhibitor was specifically engineered to bind the MALT1 catalytic site, this result concurs with what has been shown in the literature [58]. Although an IC_{50} was not calculated, the

peptide was shown to inhibit cell growth and MALT1 activity with nanomolar efficacy [2, 3].

Another result that can be taken from these data is that MI-2, even at the highest concentration of compound, is not able to fully inhibit MALT1 enzyme. The dose response curves for mepazine and z-VRPR-Fmk have minimum raw values around 100, whereas the raw values for MI-2 never dip below 500. This phenomenon could be elucidated by a few combining factors, including poor solubility, aggregation, or interference with the fluorophore in the assay. Another possibility could be that a small population of enzyme in the assay well is unable to bind compounds, regardless of potency. This population of protein could be modified differently or be folded incorrectly. The incomplete inhibition and gradual slope of MI-2, compared to the complete inhibition and steeper slope of mepazine could point towards a difference in the mechanism of action of the two inhibitors. This is supported by the literature, as mepazine is an allosteric reversible inhibitor and MI-2 is an irreversible and competitive inhibitor of MALT1's protease function [2].

The inhibitors mepazine, MI-2, and z-VRPR-Fmk showed reproducible dose response curves that were sigmoidal in shape and had small error between duplicates. Analysis of the inhibitors thioridazine and β-Lapachone show dose-response curves that are not sigmoidal and have large error between duplicates. The dose dependent inhibition of MALT1 using thioridazine or β-Lapachone is not as clear as the dose response curves of the other three inhibitors. This could be due to poor solubility, interference with the fluorophore, aggregation, or other unknown issues. Although

the IC_{50} values that were calculated with the two inhibitors indicate mildly efficacious inhibition of MALT1, the variation that is seen between and within experiments could introduce an uncontrollable variable into future experiments. The inhibitors do not reliably inhibit MALT1 in a dose-dependent manner in vitro, so they will unquestionably have lower efficacy in a cell culture or in vivo model than the other more reliable inhibitors. For these reasons, the MALT1 inhibitors mepazine, MI-2, and z-VRPR-Fmk were chosen to be investigated further in future assays.

Thermal Melt of MALT1 and Inhibitors

In order to determine if compounds bind directly to MALT1 enzyme, a thermal shift assay was used. When a protein is denatured by exposure to heat, hydrophobic pockets become exposed as the protein unfolds. SYPRO Orange dye binds these pockets and fluoresces. The fluorescent readout can be analyzed to produce a melting curve. Upon compound binding with protein, sometimes a shift in melting temperature is observed. This may be due to thermal stabilization of the protein upon compound binding. Ideally, a shift in the melting temperature of MALT1 with a compound would support the hypothesis that the inhibitors are binding MALT1 directly. If no shift in melting temperature is seen, it does not rule out the possibility that the compounds are binding protein. This experiment serves to validate the compounds and ensure that as long as the compounds are able to get into the cell, they will bind MALT1.

First, optimal assay buffer and proteins of different origins were investigated. Included in the experiment were two different assay buffers, MALT1 assay buffer

(containing Tris HCl, sodium citrate, CHAPS, BSA, EGTA, DTT) or PBS + DTT. MALT1 full length protein (Origene) was analyzed. Various stages of the analysis can be seen, including the derivative of the buffers only [R' (t)], dissociation curve of the buffers with MALT1 full length protein [R' (t)], and the negative dissociation curve of PBS buffer with and without MALT1 full length protein [-R (t)]. Ideally, the buffer should have no inherent fluorescence upon heating or this would interfere with the observance of a melting curve. The MALT1 assay buffer without MALT1 protein appears to have its own thermal melt signature, most likely due to the BSA protein present in the buffer. Unsurprisingly, when combined with MALT1 protein a similar pattern can be seen. An experiment to investigate the inherent fluorescence of two buffer components, CHAPS and BSA, was completed (data not shown). It was determined that both components contributed to the background artifact that was seen. In contrast, the PBS buffer appears to have no background fluorescence. When combined with full length MALT1 protein, a clear melting curve can be visualized, with a single peak at 50°C. From this point forward the PBS buffer was used to examine MALT1 binding with compounds via thermal shift assay.

After optimization, MALT1 inhibitors and MALT1 enzyme were tested in the thermal shift assay in order to investigate compound binding. Although a slight shift in peak fluorescence was seen with the addition of mepazine and MI-2 at 10 µM compared to the DMSO control, the replicates are not consistent within and between experiments. If further testing corroborates this result, it could indicate compound binding to MALT1. When tested without MALT1 enzyme, MI-2 exhibits fluorescence that may interfere with the assay. This can be seen at the 100 µM

concentration with MALT1 as well, suggesting that the compound may be insoluble at such a high concentration. Novel compounds A and B at 100 μM with MALT1 enzyme have melting curves that are shifted to the left. At 10 μM, however, no shift is apparent. In order for a shift in melting temperature to occur, the compound must be tested at a concentration well above their IC_{50}. Additional, the test compound should be in excess of the protein. It is possible that a shift was not seen with compounds A and B because the compounds are not potent enough to bind all of the enzyme present with the concentration used.

Compound binding with MALT1 is not apparent with these data, however, data from the biochemical assay described in "Biochemical Characterization of MALT1 inhibitors" suggests that the compounds bind and inhibit MALT1. It appears that MI-2 and mepazine may stabilize the protein, resulting in a slight increase in melting temperature. An important fact to take into account is that sodium citrate is crucial for MALT1 activity and the formation of its active confirmation in vitro [59, 60]. It is possible that the compounds are unable to bind MALT1 without sodium citrate present. By adding sodium citrate to the PBS buffer, a shift in melting temperature of MALT1 may be seen. This would indicate compound binding with the physiologically relevant confirmation of MALT1.

Protein Analysis

A panel of CLL, DLBCL, and AML cell lines was analyzed for expression of various proteins involved in NF-κB signaling. Cell lysates were probed for MALT1 and BTK, two proteins that are essential for the propagation of signaling downstream

of the BCR. CLL and DLBCL cell lines, including MEC-1, OCI-LY-3, SU-DHL-6, and U-2932, had robust expression of BTK. These cell lines also had high expression of MALT1, with the exception of the GCB-DLBCL cell line, SU-DHL-6. Since MALT1 and BTK are two protein targets of interest for small molecule inhibition, it is crucial that the cell lines being analyzed express the proteins. The AML cell lines OCI-AML-2 and OCI-AML-3 had lower expression of these proteins. Low expression of MALT1 and BTK may correlate with low levels of activation of the pathway in the specific cell lines. Typically when cell growth is reliant on constitutively active BCR signaling, high expression of NF-κB pathway component proteins is seen. The low expression of these proteins compared to cell lines with known reliance on the pathway suggests that the AML cells may not be dependent on NF-κB signling for survival, which is supported by the literature [19, 29]**.** It is therefore expected that a MALT1 or BTK inhibitor would be less efficacious at slowing the growth of these cells. It is possible that the low levels of protein present may be highly active, in which case a large amount of RelB or CYLD would be cleaved. Since this was not seen it is unlikely that the low level of MALT1 present in AML cells has high activity. Expression of the MALT1 substrates RelB and CYLD was examined. Both full length and cleaved RelB and CYLD can be seen with MEC-1, U-2932, and OCI-LY-3 cells. CYLD and RelB full length can be seen in the AML cell lines, but not the cleavage product band at 55 kDa. This result suggests that a low level of active MALT1 is present in these cells, and inhibition of MALT1 may not be effective at inhibiting cell growth. BTK inhibition may still be effective in

slowing cell growth however, as BTK is involved in the activation of pathways other than NF-κB.

Because of the robust activation of NF-κB and MALT1 in OCI-LY-3 cells, they were selected for further analysis to investigate the effect of MALT1 inhibitors on RelB cleavage. Upon cleavage by MALT1, RelB is inactivated and NF-κB proteins are free to migrate into the nucleus, thus enhancing the NF-KB signal. Theoretically, if MALT1 is inhibited, less RelB will be cleaved and a decrease in the cleavage product at 55 kDa will be seen. After cleavage by MALT1, RelB-CP is degraded by the proteosome. A proteosome inhibitor, MG-132, was used in order to stabilize the protein for detection by western blot. As expected, the addition of MG-132 appears to stabilize the cleavage product at 55 kDa. This conclusion is drawn from the fact that both lanes containing MG-132 have bands at 55 kDa whereas the cell lysates without MG-132 do not. Inhibition of MALT1 using mepazine does not appear to have a large effect on RelB-CP. There is, however, an increase in band intensity of RelB-FL at 70 kDa with the addition of mepazine. It is possible that by inhibiting MALT1, less RelB was cleaved and therefore more RelB-FL accumulated in the cell. This suggests that mepazine successfully inhibited MALT1's protease function and the cleavage of RelB, as described in the literature [3, 40]. A longer incubation time with compound + MG-132 may be necessary to induce a decrease in the amount of RelB-CP protein. It may be that a longer period of time is necessary to allow the breakdown of RelB-CP that was formed before inhibition of MALT1 by mepazine prevented cleavage, especially in the presence of MG-132. Examination of

the effect of novel MALT1 inhibitors on downstream targets, such as RelB, will be useful in the determination of compound efficacy. Even if compounds are able to bind MALT1 with a high affinity and inhibit its activity, the efficacy may be compromised if the compound is unable to inhibit cleavage of RelB and other substrates, as this is a role of MALT1 that is crucial for tumor cell survival. This assay would be useful in analyzing the effect of MALT1 inhibition in other cell lines of interest.

Inhibition of Cell Proliferation

In order to determine if MALT1 inhibitors or the commercially available BTK inhibitor Ibrutinib have an effect on cell growth and proliferation, a cell-based assay to monitor ATP was performed. The assay will provide crucial information about the specific inhibitors and how they interfere with pathways that are essential for cell survival. The analysis of each inhibitor singly in different leukemia and lymphoma subtype cell lines is critical to this study. Comparison of this experimental data to the analysis of protein expression within the cells will allow for an expansion of knowledge about the activation of certain pathways in each cell line and the reliance of the cell lines on those pathways for survival.

Using CTG reagent, the amount of ATP in each well was quantified and analyzed. Optimization of the assay included selection of an ideal time point and cell number per well. Depending on the specific cell line's size and doubling time, a different concentration was required for each cell line. A titration of cells was plated and analyzed at 1, 2, and 3 days. This allowed for the examination of each cell

concentration over time. A concentration was chosen for each cell line that allowed for the minimum number of cells per well and at least a 2-fold increase in luminescence over 2 days. The time point and cell number was also chosen so that cells were still in logarithmic phase growth over three days.

After optimization of the assay conditions, different cell lines with dilutions of single inhibitors were incubated for 3 days and analyzed. The most common trend that was seen among cell lines was the higher efficacy of Ibrutinib compared to mepazine. This was seen in the CLL cell line, MEC-1, and both DLBCL cell lines, SU-DHL-6 and OCI-LY-3. In the two AML cell lines HL-60 and OCI-AML-3 MI-2 was effective at inhibiting growth, even though MALT1 is not highly expressed in the cells. This may suggest MI-2 inhibiting cell growth through another mechanism that has nothing to do with MALT1. Ibrutinib and mepazine inhibited growth with lower efficacy than MI-2.

It is surprising that mepazine and MI-2, MALT1 inhibitors with similar potency in the fluorescent peptide cleavage assay, behaved differently in the cell based proliferation assay. This could be explained by many factors, including poor solubility or weak binding to MALT1. The mechanisms of binding of mepazine and MI-2 to MALT1 are different, which could also contribute to the higher efficacy of MI-2 in the cell based assay than mepazine. Originally discovered as a dopamine D2 receptor antagonist, mepazine has been shown to have off-target effects, causing extrapyrimidal side effects and possibly binding proteins such as Akt that have similar motifs to MALT1 [3, 44]. Especially when cells are reliant on MALT1 for

propagation of the NF-κB signal and tumor cell survival, inhibition of MALT1 specifically is crucial for cell death. The targeting of multiple proteins within the cell and not MALT1 alone would negatively impact the efficacy of mepazine in the cell lines that are heavily reliant on the pathway. This promiscuity may allow mepazine to effectively inhibit growth in cell lines not reliant on MALT1 such as GCB-DLBCL and AML cell lines by targeting other pathways.

MI-2 binds specifically and irreversibly to MALT1 at the catalytic site, which is different than the allosteric and reversible binding of mepazine. This difference could contribute to the low potency of mepazine and high potency of MI-2 in cell based assays compared to biochemical analysis. The long incubation time of the assay may contribute to this effect. The irreversible inhibitor MI-2 is permanently bound to the enzyme, inhibiting activity for the length of the assay, whereas the reversible inhibitor mepazine may transiently bind MALT1, decreasing the observed effect of the inhibitor over the three day period. Interestingly, Fontan and colleagues noted that MI-2 had greater potency in cell based assays than in biochemical analysis which corroborates the data seen here [2]. They speculate that this could be due to accumulation of the compound within cells and/or the irreversible binding to MALT1.

There are many additional variables to consider when investigating the effect of inhibitors on cells versus looking simply at inhibition of enzyme activity in a biochemical assay. Compound permeability, interaction with other agents inside and

outside the cell, and weak target binding are just some of the many variables that may play a role in decreased compound efficacy in cell-based assays.

The DLBCL and CLL cell lines are reliant on BCR signaling for cell survival [30, 32, 43, 51, 54]. BTK and MALT1 are essential for the propagation of signaling downstream of the BCR. As expected, the growth of DLBCL and CLL cell lines was affected by inhibition of BTK or MALT1. Ibrutinib is a small molecule that was thoroughly developed for optimal BTK binding before it became commercially available. Mepazine, however, was not developed or changed in any way to increase binding efficacy to MALT1. For this reason it is unsurprising that Ibrutinib was more successful in inhibiting cell growth than mepazine. This result indicates that inhibition of MALT1 in these cell lines using a potent and optimized small molecule inhibitor could effectively slow the growth of the cells.

Combination MALT1 and BTK inhibition could be efficacious at slowing the growth of CLL tumors, as well as other lymphoma and leukemia subtypes. An experiment was designed to analyze possible synergistic effects between mepazine and Ibrutinib in vitro. A matrix of compound serial dilutions was plated and analyzed for their effect on cell growth. The acquired data was analyzed using the highest single agent or Bliss additivism models to predict the percent inhibition for non-synergistic effects. The predicted percent was compared to the observed effect, and any excess over the predicted value was noted. A few conditions for each cell line and analysis method indicate only a modest synergistic effect between the two compounds. OCI-LY-3 cells with 11 µM of mepazine and 11 µM of Ibrutinib show

approximately 30% excess over the value predicted by the highest single agent model. SU-DHL-6 cells with 11 µM of mepazine and 0.4 µM of Ibrutinib show approximately 25% excess over the value predicted by the highest single agent model. Greater than 50% excess over the predicted value would ideally suggest that synergy is present between compounds.

When a dilution of Ibrutinib with and without mepazine at 11 µM was examined, it became apparent that the addition of a MALT1 inhibitor increased the efficacy of Ibrutinib. With the addition of mepazine, the IC_{50} of Ibrutinib was decreased considerably in both cell lines. When administered simultaneously, less Ibrutinib and mepazine is required to achieve the same degree of inhibition observed with a single agent. With the addition of 11 µM mepazine, approximately 60% less Ibrutinib is needed to achieve 50% inhibition of OCI-LY-3 cell growth. Similarly with the addition of 11 µM mepazine, approximately 80% less Ibrutinib is needed to achieve 50% inhibition of SU-DHL-6 cell growth. Although more testing is needed to confirm or deny synergy between mepazine and Ibrutinib, there is reason to think that combinatorial treatment may be beneficial for some patients regardless of the presence of a synergistic effect. The addition of a MALT1 inhibitor to BTK inhibition therapy may overcome the many downstream activating mutations that have been shown to confer resistance to BTK inhibitors.

Future Experiments

In the future, there are many possible experiments that would allow for the expansion of knowledge on MALT1 inhibitors, combination therapy with BTK

inhibitors, and the effect of MALT1 inhibition on pathway activation and cell growth of CLL, DLBCL, and AML cells. Investigation of the effect of MALT1 inhibition on MALT1's scaffold function would be useful for analyzing novel compound effectiveness. This could be completed simply by looking at the phosphorylation of IKK, a crucial step in the propagation of classical NF-κB directly downstream of MALT1. Successful transfection of suspension cell lines is important for the future of the project. Plasmid DNA, siRNA, or shRNA would be useful tools for investigating compound specificity, efficacy, or pathway activation in the cells. An NF-κB reporter plasmid would allow for direct quantification of NF-κB activity with and without inhibition of MALT1 or BTK. Knockdown of MALT1 or BTK using siRNA or shRNA would allow for analysis of compound specificity. Creation of a stable cell line using MALT1 shRNA would allow for analysis of compound specificity. Inhibition of cell growth in MALT1 knockdown cells indicates that the compound is inhibiting growth through inhibition of a different protein. Ultimately, analysis of cell growth and pathway activation is crucial for the development and optimization of a novel MALT1 inhibitor. Secondary cell-based assays will serve to analyze compound effects on MALT1 inhibition in a more physiologically relevant environment than a biochemical assay.

Summary and Conclusions

Biochemical characterization of seven MALT1 inhibitors was completed using a novel fluorescent peptide cleavage assay. Reliable dose-dependent inhibition of MALT1 enzyme could be seen with five out of the seven inhibitors (mepazine, MI-2, and z-VRPR-Fmk, compound A, compound B), prompting further investigation of these inhibitors as tool compounds. A thermal melting experiment was completed and preliminary results suggest that MI-2 and mepazine bind MALT1. Further optimization of this assay is necessary to confirm the results, however.

In order to determine if MALT1 inhibition is efficacious at slowing the growth of CLL, AML, and DLBCL cells, a panel of cell lines was analyzed for various proteins downstream of BCR activation. The results indicate that a CLL cell line (MEC-1), and two ABC-DLBCL cell lines (U-2932 and OCI-LY-3) have high expression of many proteins in the NF-κB signaling pathway. High expression of these proteins may indicate robust activation of the pathway within these cells, suggesting that a potent inhibitor of proteins in the pathway would be efficacious in slowing growth of the cells. The AML cell lines (OCI-AML-2, OCI-AML-3, HL-60) have low expression of many of these proteins, but high expression of BTK. In cell proliferation assays, the MALT1 inhibitors mepazine and MI-2 and the BTK inhibitor Ibrutinib were shown to inhibit cell growth in a dose-dependent manner. Each cell line

showed a different response to each inhibitor and trends among cell types were seen. Observed trends included high efficacy of MI-2 at inhibiting AML cell growth and high efficacy of Ibrutinib at inhibiting DLBCL and CLL cell growth. Combinatorial studies indicate that synergy between Ibrutinib and mepazine may exist. Further experimentation is needed to confirm this effect, although combination treatment with a clinical MALT1 inhibitor and Ibrutinib may be effective despite a lack of synergy.

Cells were successfully transfected with siRNA and plasmid DNA by electroporation. This could be used in the future to create a stable cell line expressing an NF-κB reporter plasmid. This will be useful in the direct examination of the effect MALT1 inhibitors on its effector functions downstream. Transfection of the cells with siRNA directed at MALT1 and/or BTK would shed light on the activation of certain pathways and the existence of certain mutations in each cell line and cell subtype. The effect of knockdown of MALT1 or BTK could be compared to the effect seen with chemical inhibitors in order to clarify compound mechanisms of binding and enhance the optimization of compound SAR knowledge.

Ultimately, the development of a novel MALT1 small molecule inhibitor would be highly efficacious in treating B-cell malignancies such as ABC-DLBCL. This research indicates that a MALT1 inhibitor could also be effective at treating patients with CLL. Combination therapy with MALT1 and

BTK inhibitors may be effective at treating patients with CLL, especially those who develop activating mutations downstream of BTK, thus rendering BTKi therapy ineffective. Addition of a MALT1 inhibitor to BTKi therapy could prevent this resistance by simultaneously inhibiting a protein within the same pathway downstream of the activating mutation. A future direction of this project should focus on comparison of chemical inhibition of MALT1 and BTK to knockdown using siRNA to further elucidate activated pathways in each cell line and the effect on cell growth and phenotype. Another focus should be the optimization of thermal shift assay to ensure compound binding to MALT1 and investigation of CARD11 mutants in DLBCL and CLL patients and the effect on BTKi resistance.

References

1. Fontan, L. and A. Melnick, *Molecular pathways: targeting MALT1 paracaspase activity in lymphoma.* Clin Cancer Res, 2013. **19**(24): p. 6662-8.

2. Fontan, L., et al., *MALT1 small molecule inhibitors specifically suppress ABC-DLBCL in vitro and in vivo.* Cancer Cell, 2012. **22**(6): p. 812-24.

3. Nagel, D., et al., *Pharmacologic inhibition of MALT1 protease by phenothiazines as a therapeutic approach for the treatment of aggressive ABC-DLBCL.* Cancer Cell, 2012. **22**(6): p. 825-37.

4. Lim, S.M., et al., *Identification of beta-Lapachone Analogs as Novel MALT1 Inhibitors To Treat an Aggressive Subtype of Diffuse Large B-Cell Lymphoma.* J Med Chem, 2015. **58**(21): p. 8491-502.

5. Honigberg, L.A., et al., *The Bruton tyrosine kinase inhibitor PCI-32765 blocks B-cell activation and is efficacious in models of autoimmune disease and B-cell malignancy.* Proc Natl Acad Sci U S A, 2010. **107**(29): p. 13075-80.

6. Hailfinger, S., G. Lenz, and M. Thome, *Targeting B-cell lymphomas with inhibitors of the MALT1 paracaspase.* Curr Opin Chem Biol, 2014. **23**: p. 47-55.

7. Roskoski, R., Jr., *Ibrutinib inhibition of Bruton protein-tyrosine kinase (BTK) in the treatment of B cell neoplasms.* Pharmacol Res, 2016. **113**(Pt A): p. 395-408.

8. *SEER Cancer Statistics Factsheers: Leukemia.* National Cancer Institute, 2016.

9. *SEER Cancer Statistic Factsheets: Acute Myeloid Leukemia.* National Cancer Institute, 2016.

10. *SEER Cancer Statistics Factsheets: Chronic Lymphocytic Leukemia.* National Cancer Institute, 2016.

11. Institute, N.C. *A Snapshot of Leukemia*. 2014.

12. Byrd, J.C., et al., *Targeting BTK with ibrutinib in relapsed chronic lymphocytic leukemia.* N Engl J Med, 2013. **369**(1): p. 32-42.

13. Brown, J.R., *Ibrutinib (PCI-32765), the first BTK (Bruton's tyrosine kinase) inhibitor in clinical trials.* Curr Hematol Malig Rep, 2013. **8**(1): p. 1-6.

14. Burger, J.A. and J.J. Buggy, *Bruton tyrosine kinase inhibitor ibrutinib (PCI-32765).* Leuk Lymphoma, 2013. **54**(11): p. 2385-91.

15. Maddocks, K. and J.A. Jones, *Bruton tyrosine kinase inhibition in chronic lymphocytic leukemia.* Semin Oncol, 2016. **43**(2): p. 251-9.

16. Burger, J.A., et al., *Clonal evolution in patients with chronic lymphocytic leukaemia developing resistance to BTK inhibition.* Nat Commun, 2016. **7**: p. 11589.

17. Spaargaren, M., et al., *BTK inhibitors in chronic lymphocytic leukemia: a glimpse to the future.* Oncogene, 2015. **34**(19): p. 2426-36.

18. Woyach, J.A. and A.J. Johnson, *Targeted therapies in CLL: mechanisms of resistance and strategies for management.* Blood, 2015. **126**(4): p. 471-7.

19. Rushworth, S.A., et al., *Identification of Bruton's tyrosine kinase as a therapeutic target in acute myeloid leukemia.* Blood, 2014. **123**(8): p. 1229-38.

20. Blankart, C.R., et al., *Cost of illness and economic burden of chronic lymphocytic leukemia.* Orphanet J Rare Dis, 2013. **8**: p. 32.

21. Oppezzo, P. and G. Dighiero, *"Role of the B-cell receptor and the microenvironment in chronic lymphocytic leukemia".* Blood Cancer J, 2013. **3**: p. e149.

22. Redaelli, A., et al., *Economic burden of acute myeloid leukemia: a literature review.* Cancer Treat Rev, 2004. **30**(3): p. 237-47.

23. Zeidan, A.M., et al., *Economic burden associated with acute myeloid leukemia treatment.* Expert Rev Hematol, 2016. **9**(1): p. 79-89.

24. *Cancer Stat Facts: Non-Hodgkin Lymphoma.* National Cancer Institute, 2016.

25. Slawsky, K.A., *Economic burden of relapsed/refractory diffuse large B-cell non-Hodgkin's lymphoma (DLBCL): A review of the literature.*, in *J Clin Oncol*. 2010.

26. Kutikova, L., et al., *Medical costs associated with non-Hodgkin's lymphoma in the United States during the first two years of treatment.* Leuk Lymphoma, 2006. **47**(8): p. 1535-44.

27. Kuppers, R., *Mechanisms of B-cell lymphoma pathogenesis.* Nat Rev Cancer, 2005. **5**(4): p. 251-62.

28. Stevenson, F.K., et al., *B-cell receptor signaling in chronic lymphocytic leukemia.* Blood, 2011. **118**(16): p. 4313-20.

29. De Kouchkovsky, I. and M. Abdul-Hay, *'Acute myeloid leukemia: a comprehensive review and 2016 update'.* Blood Cancer J, 2016. **6**(7): p. e441.

30. Fowler, N. and E. Davis, *Targeting B-cell receptor signaling: changing the paradigm.* Hematology Am Soc Hematol Educ Program, 2013. **2013**: p. 553-60.

31. Lenz, G., et al., *Oncogenic CARD11 mutations in human diffuse large B cell lymphoma.* Science, 2008. **319**(5870): p. 1676-9.

32. Davis, R.E., et al., *Chronic active B-cell-receptor signalling in diffuse large B-cell lymphoma.* Nature, 2010. **463**(7277): p. 88-92.

33. Lenz, G., et al., *Molecular subtypes of diffuse large B-cell lymphoma arise by distinct genetic pathways.* Proc Natl Acad Sci U S A, 2008. **105**(36): p. 13520-5.

34. Song, G., G. Ouyang, and S. Bao, *The activation of Akt/PKB signaling pathway and cell survival.* J Cell Mol Med, 2005. **9**(1): p. 59-71.

35. Hachmann, J., et al., *Probes to monitor activity of the paracaspase MALT1.* Chem Biol, 2015. **22**(1): p. 139-47.

36. Hailfinger, S., A. Schmitt, and K. Schulze-Osthoff, *The paracaspase MALT1 dampens NF-kappaB signalling by cleaving the LUBAC subunit HOIL-1.* FEBS J, 2016. **283**(3): p. 400-2.

37. Staudt, L.M., *Oncogenic activation of NF-kappaB.* Cold Spring Harb Perspect Biol, 2010. **2**(6): p. a000109.

38. Pahl, H.L., *Activators and target genes of Rel/NF-kappaB transcription factors.* Oncogene, 1999. **18**(49): p. 6853-66.

39. Staal, J., T. Bekaert, and R. Beyaert, *Regulation of NF-kappaB signaling by caspases and MALT1 paracaspase.* Cell Res, 2011. **21**(1): p. 40-54.

40. Hailfinger, S., et al., *Malt1-dependent RelB cleavage promotes canonical NF-kappaB activation in lymphocytes and lymphoma cell lines.* Proc Natl Acad Sci U S A, 2011. **108**(35): p. 14596-601.

41. Uehata, T., et al., *Malt1-induced cleavage of regnase-1 in CD4(+) helper T cells regulates immune activation.* Cell, 2013. **153**(5): p. 1036-49.

42. Jeltsch, K.M., et al., *Cleavage of roquin and regnase-1 by the paracaspase MALT1 releases their cooperatively repressed targets to promote T(H)17 differentiation.* Nat Immunol, 2014. **15**(11): p. 1079-89.

43. Schneider, C., L. Pasqualucci, and R. Dalla-Favera, *Molecular pathogenesis of diffuse large B-cell lymphoma.* Semin Diagn Pathol, 2011. **28**(2): p. 167-77.

44. Ohlow, M.J. and B. Moosmann, *Phenothiazine: the seven lives of pharmacology's first lead structure.* Drug Discov Today, 2011. **16**(3-4): p. 119-31.

45. Akinleye, A., et al., *Ibrutinib and novel BTK inhibitors in clinical development.* J Hematol Oncol, 2013. **6**: p. 59.

46. Hendriks, R.W., *Drug discovery: New Btk inhibitor holds promise.* Nat Chem Biol, 2011. **7**(1): p. 4-5.

47. Wu, H., et al., *Ibrutinib selectively targets FLT3-ITD in mutant FLT3-positive AML.* Leukemia, 2016. **30**(3): p. 754-7.

48. Herman, S.E., et al., *Bruton tyrosine kinase represents a promising therapeutic target for treatment of chronic lymphocytic leukemia and is effectively targeted by PCI-32765.* Blood, 2011. **117**(23): p. 6287-96.

49. Ponader, S., et al., *The Bruton tyrosine kinase inhibitor PCI-32765 thwarts chronic lymphocytic leukemia cell survival and tissue homing in vitro and in vivo.* Blood, 2012. **119**(5): p. 1182-9.

50. Maddocks, K. *A Phase 2 Study of the Bruton's Tyrosine Kinase (Btk) Inhibitor, PCI-32765(Ibrutinib), in Relapsed and Refractory Patients With Chronic Lymphocytic Leukemia (CLL)/Small Lymphocytic Lymphoma (SLL) and B-cell Prolymphocytic Leukemia (B-PLL)*. Clinicaltrials.gov 2015; Available from: https://clinicaltrials.gov/ct2/show/NCT01589302?term=ibrutinib&rank=28.

51. Messina, M., et al., *Genetic lesions associated with chronic lymphocytic leukemia chemo-refractoriness.* Blood, 2014. **123**(15): p. 2378-88.

52. Helena Peilot Sjogren, L.R., Pia Hansson, Elisabeth Back, Tyrrell Norris, Robert Roth, Helen Boyd, *Development of a Cell Based Assay to Screen for Inhibition of MALT1 Protease Activity*, in *ELRIG- Advances in Cell Based Screening in Drug Discovery*. 2015: Astra Zeneca Molndal, Sweden.

53. Fredrik Öberg, S.K., Ian Henderson, Ellen Hewitt, Anders Kallin, Susanne Sedig, Jimmy Lindberg, Anna-Karin, *Development of selective small-molecule inhibitors of cellular MALT1 protease activity*, in *American Association for Cancer Research*. 2016.

54. Abdel-Magid, A.F., *MALT1 Inhibitors May Potentially Treat Lymphomas and Autoimmune Disorders.* ACS Med Chem Lett, 2016. **7**(3): p. 205-6.

55. Pelzer, C., et al., *The protease activity of the paracaspase MALT1 is controlled by monoubiquitination.* Nat Immunol, 2013. **14**(4): p. 337-45.

56. Borisy, A.A., et al., *Systematic discovery of multicomponent therapeutics.* Proc Natl Acad Sci U S A, 2003. **100**(13): p. 7977-82.

57. Mohamed, A.J., et al., *Bruton's tyrosine kinase (Btk): function, regulation, and transformation with special emphasis on the PH domain.* Immunol Rev, 2009. **228**(1): p. 58-73.

58. Ferch, U., et al., *Inhibition of MALT1 protease activity is selectively toxic for activated B cell-like diffuse large B cell lymphoma cells.* J Exp Med, 2009. **206**(11): p. 2313-20.

59. Wiesmann, C., et al., *Structural determinants of MALT1 protease activity.* J Mol Biol, 2012. **419**(1-2): p. 4-21.

60. Hachmann, J., et al., *Mechanism and specificity of the human paracaspase MALT1.* Biochem J, 2012. **443**(1): p. 287-95.

61. Corporation, P., *Technical Bulletin: CellTiter-Glo® Luminescent Cell Viability Assay*. 2015.

Abbreviations

A20- (also known as Tumor Necrosis Factor, Alpha-Induced Protein 3- TNFAIP3)
ABC- Activated B-Cell-like
AKT- (also known as PKB- Protein Kinase B)
ALL- Acute Lymphoblastic Leukemia
AML- Acute Myeloid Leukemia
AP-1- Activator Protein 1
ATCC- American Type Culture Collection
BCA- Bicinchoninic Acid
BCL-10- B-Cell Lymphoma Protein 1
BCR- B-Cell Receptor
BIRC3- Baculoviral IAP Repeat- Containing Protein 3
BSA- Bovine Serum Albumin
BTK- Bruton's Tyrosine Kinase
BTKi- Bruton's Tyrosine Kinase Inhibitor
CARD11/CARMA1- Caspase recruitment domain-containing protein 11/ Caspase Recruitment Domain Containing-Membrane Associated Guanylate Kinase-like Domain 1
CBM- CARD11-BCL-10-MALT1
CD-Cluster of Differentiation
CEBPA- CCAAT/Enhancer-Binding Protein Alpha
CFP- Cyan Fluorescent Protein
CHAPS- 3-[(3-cholamidopropyl)dimethylammonio]-1-propanesulfonate
CHOP chemotherapy- Cyclophosphamide, Hydroxydaunorubicin (also known as doxorubicin or adriamycin), Oncovin (also known as vincristine), and Prednisone
c-KIT- c-Kit Hardy-Zuckerman 4 Feline Sarcoma Viral Oncogene Homolog (also known as Mast/Stem Cell Growth Factor Receptor (SCFR) or CD117)
CLL-Chronic Lymphocytic Leukemia
CsiRNA- control siRNA
CTG- Cell Titer- Glo
Ctla4- Cytotoxic T-Lymphocyte-Associated Protein 4
CXCL12- C-X-C Motif Chemokine 12 (also known as Stromal Cell Derived Factor-1)
CYLD- Cylindromatosis
DAG- Diacylglycerol
DD- Death Domain
DLBCL- Diffuse Large B-Cell Lymphoma
DMEM- Dulbecco's Modified Eagle Medium

DMSO- Dimethyl Sulfoxide
DNA- Deoxyribonucleic Acid
DNMT3A- DNA (cytosine-5)-Methyltransferase 3A
DSMZ- German Collection of Microorganisms and Cell Cultures
DTT- Dithiothreitol
ELISA- Enzyme Linked Immunosorbent Assay
ERK- Extracellular Signal-Regulated Kinase
FBS- Fetal Bovine Serum
FcγRIII- Low Affinity Immunoglobulin Receptor Gamma 3
FLT3- Fms-Like Tyrosine Kinase 3 (also known as CD135)
FRET- Fluorescence Resonance Energy Transfer
GAPDH- Glyceraldehyde Phosphate Dehydrogenase
GCB- Germinal Center B-Cell-like
HAS- Highest Single Agent
HRP- Horseradish Peroxidase
HTS- High Throughput Screening
IBTK- Inhibitor of Bruton's Tyrosine Kinase
IC_{50}- Half Maximal Inhibitory Concentration
Icos- Inducible T-Cell Costimulator (also known as CD278)
IDH-1/2- Isocitrate Dehydrogenase 1/2
Ig- Immunoglobulin
IgV- Immunoglobulin Variable
IKK- Inhibitor of Kappa B Kinase
IL- Interleukin
IP_3- Inositol-1,4,5-triphosphate
ITAM- Immune Receptor Tyrosine Activation Motif
IκB-α- Inhibitor of κB Alpha
JNK- c-Jun N-Terminal Kinase
kDa- kilodalton
KRAS- Kirsten Rat Sarcoma Viral Oncogene Homolog
Lyn- Lck/Yes Novel Tyrosine Kinase
MALT1- Mucosa-Associated Lymphoid Tissue 1
MAPK- Mitogen Activated Protein Kinase
MCL- Mantle Cell Lymphoma
MEM- Minimum Essential medium
mRNA- messenger Ribonucleic Acid
mTOR- Mechanistic Target of Rapamycin
MYC- Myelocytomatosis Oncogene
MyD88- Myeloid Differentiation Primary Response Gene 88

NF-κB- Nuclear Factor Kappa Light Chain Enhancer of Activated B Cells
NHL-Non-Hodgkin's Lymphoma
Notch1- Notch Homolog 1
NPM1- Nucleophosmin (also known as Nucleolar Phosphoprotein B23 or Numatrin)
NRAS- Neuroblastoma Rat Sarcoma Viral Oncogene Homolog
PBS- Phosphate Buffered Saline
p-BTK- Phospho-Bruton's Tyrosine Kinase
PH- Pleckstrin Homology
PI3K- Phosphatidylinositol-4,5-bisphosphate 3-kinase
PIP_3- Phosophatidylinositol-3,4,5-triphosphate
p-IκB-α- Phospho- Inhibitor of Kappa B Alpha
PKC- Protein Kinase C
PLCγ2- 1-Phosphatidylinositol-4,5-bisphosphate Phosphodiesterase Gamma-2
PMBL- Primary Mediastinal B-Cell like
PTEN- Phosphatase and Tensin Homolog
PVDF- Polyvinylidene Fluoride
qRT-PCR- Quantitative Real Time Polymerase Chain Reaction
RANK- Receptor Activator of Nuclear Factor Kappa B
Rap1- Ras-related Protein 1
Ras- Rat Sarcoma Viral Oncogene Homolog
RCF- Relative Centrifugal Force
RelB-CP- RelB-Cleavage Product
RelB-FL- RelB- Full Length
RIPA- Radioimmunoprecipitation
RLU- Relative Luminescence Units
RPMI- Roswell Park Memorial Institute Medium
SDS- PAGE- Sodium Dodecyl Sulfate Polyacrylamide Gel Electrophoresis
SF3B1- Splicing Factor 3B Subunit 1
SH1/TK- Src Homology 1/ Tyrosine Kinase
SH2- Scr Homology 2
SH3- Src Homology 3
shRNA- Short Hairpin RNA
siRNA- short interfering RNA
STAT3- Signal Transducer and Activator of Transcription 3
SYK- Spleen Tyrosine Kinase
TBS-T- Tris Buffered Saline with Tween 20
TCR- T-Cell Receptor
TET2- Tet Methylcytosine Dioxygenase 2
TH- Tec Homology

TLR- Toll-Like Receptor
TNF- Tumor Necrosis Factor
TP53- Tumor Protein p53
TRAF-6- TNF-Receptor Associated Factor 6
UTR- Untranslated Region
WR- Working Reagent
XLA- X-Linked agammaglobulinemia
YFP- Yellow Fluorescent Protein
Z-VRPR-Fmk- Z-Val-Arg-Pro-DL-Arg-Fluoromethylketone

Attributes

Figure 1- This image was taken from "Molecular pathways: targeting MALT1 paracaspase activity in lymphoma" by L. Fontan, 2013. [1]

Figure 2- Images were taken from "Targeting B-cell lymphomas with inhibitors of the MALT1 paracaspase" by S. Hailfinger, 2014 and "Ibrutinib inhibition of Bruton protein-tyrosine kinase (BTK) in the treatment of B cell neoplasms" by B. Roskoski, 2016 and compiled by Christina Snyder. [6, 7]

Figure 3- Images were taken from "The Bruton tyrosine kinase inhibitor PCI-32765 blocks B-cell activation and is efficacious in models of autoimmune disease and B-cell malignancy" by L.A. Honigberg, 2010, "Pharmacologic inhibition of MALT1 protease by phenothiazines as a therapeutic approach for the treatment of aggressive ABC-DLBCL" by D. Nagel, 2012, and "MALT1 small molecule inhibitors specifically suppress ABC-DLBCL in vitro and in vivo" by L. Fontan, 2012, and compiled by Christina Snyder. [2, 3, 5]

Figure 4- This figure was created by Christina Snyder.

Figure 5- This figure was taken from Promega's Cell Titer-Glo technical bulletin. [61]

Figure 6- This figure was created by Christina Snyder.

Figure 7- The work completed to make this figure, data analysis, and compilation of the figure was completed by Christina Snyder and Dr. Rachael Siegel.

Figure 8- The work completed to make this figure, data analysis, and compilation of the figure was completed by Christina Snyder.

Figure 9- The work completed to make this figure, data analysis, and compilation of the figure was completed by Christina Snyder.

Figure 10- The work completed to make this figure, data analysis, and compilation of the figure was completed by Christina Snyder.

Figure 11- The work completed to make this figure, data analysis, and compilation of the figure was completed by Christina Snyder.

Figure 12- The work completed to make this figure, data analysis, and compilation of the figure was completed by Christina Snyder.

Figure 13- The work completed to make this figure, data analysis, and compilation of the figure was completed by Christina Snyder.

Figure 14- The work completed to make this figure, data analysis, and compilation of the figure was completed by Christina Snyder.

Figure 15- The work completed to make this figure, data analysis, and compilation of the figure was completed by Christina Snyder.

Figure 16- The work completed to make this figure, data analysis, and compilation of the figure was completed by Christina Snyder.

Figure 17- The work completed to make this figure, data analysis, and compilation of the figure was completed by Christina Snyder and Dr. Rachael Siegel.

Figure 18- The work completed to make this figure, data analysis, and compilation of the figure was completed by Christina Snyder and Dr. Rachael Siegel.

Figure 19- The work completed to make this figure, data analysis, and compilation of the figure was completed by Christina Snyder and Dr. Rachael Siegel.

Table 1- This table was created by Christina Snyder.

Table 2- This table was created by Christina Snyder.